CFD STUDY OF PARTICLE CONCENTRATION AND STOKES NUMBER EFFECT ON EROSION PROFILE

by

Wahib Mufid Salim

A Thesis presented to the Faculty of the
American University of Sharjah
College of Engineering
In Partial Fulfillment
of the Requirements
for the Degree of

Master of Science in
Mechanical Engineering

Sharjah, United Arab Emirates

April 2017

Approval Signatures

We, the undersigned, approve the Master's Thesis of Wahib Mufid Salim

Thesis Title: CFD Study of Particle Concentration and Stokes Number Effect on Erosion Profile.

Signature	**Date of Signature** (dd/mm/yyyy)
_____	_____
Dr. Basil Darras Associate Professor, Department of Mechanical Engineering Thesis Advisor	
_____	_____
Dr. Ammar Abdilghanie Senior Modeling and Simulation Engineer, MENAT Technology Team, GE Oil and Gas Thesis Co-Advisor	
_____	_____
Dr. Imran Qureshi Assistant Professor, Department of Mechanical Engineering Thesis Committee Member	
_____	_____
Dr. Mohammad AlHamaydeh Associate Professor, Department of Civil Engineering Thesis Committee Member	
_____	_____
Dr. Mamoun Abdel-Hafez Head, Department of Mechanical Engineering	
_____	_____
Dr. Mohamed El-Tarhuni Associate Dean for Graduate Affairs and Research, College of Engineering	
_____	_____
Dr. Richard Schoephoerster Dean, College of Engineering	
_____	_____
Dr. Khaled Assaleh Interim Vice Provost for Research and Graduate Studies	

Acknowledgements

First and foremost, I would like to thank The Great Lord for all His Amazing and Generous Blessings which without them I would have neither done this work nor reached this point in my career.

I would like to also thank my father, Mufid Wahib Salim, and sister, Hiba Mufid Salim, for all their support, kindness, love and warmth throughout my life.

Furthermore, I would like to hugely thank my advisors Dr. Basil Darras and Dr. Ammar Abdilghanie. They are two of the best professors I became acquainted with, whom without their patience, understanding and continuous support this work could not have been established. They have taught me to be a better researcher.

Moreover, I would like to thank the department of mechanical engineering at the American University of Sharjah for giving me the opportunity to attain my bachelor's and master's degrees, and for all their support throughout these quests.

I finally would like to thank all my family members and friends for all their help and support throughout this stage of my life.

Dedication

I dedicate this work to my late mother, Abeer Elias Saoud, who I know she would be very proud of such an achievement. She is the reason behind all my past, present and future success. May The Great Lord Rest her pious soul in peace.

To my beloved father and sister.

To my beloved country, Syria, which is currently facing difficult times. May The Great Lord Return back its peace.

Abstract

A very common problem that continuously faces industrial applications involving fluid flow is solid particle erosion. This type of erosion is caused when solid particles carried by a fluid flow continuously impact a surface thus removing some of its material. It is especially notable in pipelines, oil and gas industry, and gas turbines leading to a decline in their performance, safety, and other aspects. Consequently, it is very important to be able to predict erosion in order to prevent failure of systems, protect the environment, and reduce costs. However, erosion is controlled by many parameters, which increase the complexity of the problem. Literature tends to provide sufficient information on how these parameters affect total erosion and erosion rate. On the other hand, it does not give enough analysis about the effect on the erosion profile. Therefore, this thesis aims at performing a parametric study on the effect of solid particle concentration and Stokes number on the erosion profile of a direct jet impingement slurry flow over a ductile material. A CFD (Computational Fluid Dynamics) model was developed using ANSYS CFX software to perform the needed analysis. The Stokes number was evaluated by looking at three of its defining parameters: solid particle diameter, nozzle average velocity and fluid viscosity. Additionally, the coupled effect of solid particle concentration and Stokes number was studied. It was found that as concentration increases, the erosion profile magnitude also increases but the change in its shape tends to saturate. However, it was also found that the effect of Stokes number on magnitude and shape of the erosion profile is dependent on the level of particle concentration and which defining parameter is under investigation. At low concentration, the change in profile shape saturates with increase in Stokes number when varying the nozzle average velocity and fluid viscosity parameters; whereas, when evaluating the solid particle diameter, the shape tends to develop into a that of a high Stokes flow. However, at high concentration, the profile shape significantly grows into that of a high Stokes flow as the Stokes number increases when varying any of the three defining parameters.

Keywords: ***CFD; direct jet impingement; ductile material; slurry flow.***

Table of Contents

List of Figures

List of Tables

List of Nomenclature

Any missing symbols or variables from this list are defined directly when they first appear in their corresponding chapters.

a	Constant depending on particle and surface material properties
a_1	Constant determined by combining experimental and CFD results
A_i	Impact angle empirical constant
$b_{1,2}$	Constant determined by combining experimental and CFD results
BH	Brinell hardness of target
c	Fraction of particles cutting in an idealized manner
C	Flow stress temperature dependence constant
C_p	Heat capacity of target
Cv	Solid particle concentration by volume
Cw	Solid particle concentration by weight
d_p	Particle diameter
d_0	Threshold particle diameter below which no erosion occurs
e_t	Restitution coefficients in tangential direction
E_p	Elastic modulus of particle
E_t	Elastic modulus of target
E_e	Effective elastic modulus
f	Fraction of volume loss caused by median spalling mechanism
$F(t)$	Number of impact constant
$F(\alpha)$	Particle impact angle function
F_s	Particle shape factor
$F_{d,V}$	Fragmentation for test condition
G	Gram molecular weight of target
H_p	Hardness of particle
H_t	Hardness of target
H_V	Vickers hardness of target
I	Empirical exponent
I	Moment of inertia of single particle
k	Thermal conductivity of target

K	Velocity component normal to surface below which no erosion takes place in certain hard materials
K_c	Fracture toughness
K_p	Physical characteristics constant
K_T	Kinetic energy transferred from impacting particle to target per unit mass of particles
$K_{1,2,3,\ldots}$	Proportionality constants
L	Depth of deformation
L_v	Plastic zone volume
m_p	Mass of single particle
M	Total mass of impinging particle
n	Velocity exponent determined experimentally
n_h	Strain hardening exponent
$n_{1,2,3\ldots}$	Impact condition constant
p	Static pressure
P	Constant plastic flow stress
r	Radius of particle
R	Roundness of particle
S_M	Sum of body forces
t	Time
T	Toughness
T_m	Melting temperature
U	Nozzle average velocity
Ui, Uj, Uk	Fluctuating velocity tensor terms
V_p	Particle velocity
V_r	Residual parallel component of particle velocity at small angles of attack
V_{ref}	Standard test velocity of particle
V_0	Threshold velocity below which distortion is entirely elastic and no damage occurs
W	Proportion of sample (by weight) within specified size range after testing
W_0	Proportion of sample (by weight) within specified size range before testing

x_i, x_j, x_k	Coordinate tensor terms
$\dot{x}_t'$	Horizontal velocity of tip of particle when cutting ceases
y_t	Vertical coordinate

Greek Letters

α	Particle impact angle
α_m	Maximum erosion impact angle
α_{p0}	Impact angle at which horizontal velocity component has just become zero when particle leaves body
δ	Deformation wear factor, the amount of energy needed to remove unit volume of material
δ_{ij}	Kronecker delta function
ΔH_m	Enthalpy of melting target
ε	Turbulence dissipation rate
ε_m	Erosion rate (mass loss/impact mass)
ε_V	Erosion rate (volume loss/impact mass)
ε_{VC}	Volume of material removed by cutting mechanism
$\varepsilon_{VC1,2}$	Volumes of material removed by cutting mechanism 1and 2
ε_{VP}	Volume of material removed by single abrasive grain of mass
ε_{VT}	Total volume removal
$\widehat{\varepsilon}_1, \widehat{\varepsilon}_2$	Maximum erosion rates for velocity V_{ref}
ε_{90}	Erosion rate (volume loss/impact mass) due to normal impact
κ	Ratio of vertical to horizontal force component on particle
λ	Distance between center of mass of particle and the contact point
μ	Friction coefficient
μ_c	Critical friction coefficient
μ_f	Fluid dynamic viscosity

μ_p	Poisson coefficient of particle
μ_t	Poisson coefficient of target
ρ or ρ_f	Fluid density
ρ_p	Density of particle
ρ_t	Density of target surface
τ_{ij}	Shear stress tensor
χ	Cutting wear factor, the quantity of energy needed to scratch out unit volume from a surface
ψ	Ratio of depth of contact to depth of cut
Ω_c	Critical strain for onset of lip formation
$\Delta\Omega_m$	Mean strain increment induced by each impact

Chapter 1. Introduction

This chapter provides a brief overview of the phenomenon of solid particle erosion and its resulting negative impact on engineering systems. Then, a description of the problem investigated in this thesis is presented in addition to listing its contribution and outcome. At the end, a general organization of the whole thesis is described.

1.1. Overview

It is always an important task in engineering to increase the efficiency of systems and find solutions to existing problems. One of the main problems that currently faces many engineering systems is the concept of solid particle erosion. This phenomenon can be defined as the material removal of surfaces due to the continuous impact of solid particles carried by fluids; if the fluid is liquid then it is referred to as slurry flow whereas if it is gas, it is called dry flow [1]. Some of the engineering applications and systems that face this problem are gas turbines, boilers, fluidized beds, aircrafts operating at low altitudes, heat exchangers, oil and gas industry [1] and several others. Results of solid particle erosion can be leaks in pipelines, failure in equipment such as pumps, valves, plugged tees, elbows [1,2], and others. This in turn can result in expensive repairs, loss of production time, environmental disasters, and potential injury to surrounding personnel [1,2].

As a result, it is very important to develop ways in which solid particle erosion can be predicted in order to ensure safe operation and better performance of equipment in industry. However, Parsi et al. [2] suggested that solid particle erosion prediction is not an easy task and, despite all the work that has been done to study erosion, its mechanism is still not fully understood. Furthermore, Parsi et al. [2] explained that there are three approaches by which researchers usually follow in order to come up with erosion prediction models: empirical, CFD (Computational Fluid Dynamics)-based and mechanistic; however, a combination of these methods is usually the proposed erosion modeling in literature. Despite the controversy in understanding erosion mechanisms, there is a consensus about the corresponding controlling factors. Parsi et al. [2] and Frosell et al. [3] suggest that these factors can be grouped into four categories: fluid properties (which include fluid viscosity and density), particle properties (which include particle shape, size, hardness and density), impact properties (which include

particle impact angle and speed), and target surface properties (which describe the mechanical properties of surface under erosion).

Furthermore, looking at the erosion profile associated with flows carrying solid particles can give a lot of information about the resulting erosion shape and magnitude in equipment. However, as previously described, many parameters affect and control erosion. Thus, an investigation of the effect of these parameters is important to understand how correspondingly the erosion profile changes. This investigation is very important to help increase the life and productivity of systems associated with such flows, and thus decrease production and repair costs. For instance, understanding the relation between the erosion profile and these parameters can provide a good indication about the desirable operating condition of a system. If erosion is overestimated, this could result in operating the system at lower status, and thus decreasing its productivity and efficiency. On the other hand, if erosion is underestimated, it could lead to operating the system over its safety limit, causing it to fail. Therefore, understanding this relation is important for the efficiency and safety of an operating system. Additionally, being able to know how the erosion profile would look like with respect to a certain parameter can give a good indication of areas of high and low erosion in an equipment. This in turn gives the opportunity to further support only areas of high erosion (such as thickening their material) instead of changing the whole equipment's design, and thus reducing repair cost and prolonging its life.

1.2. Thesis Objectives

Investigating the erosion profile is very important because it gives insight into the erosion behavior and magnitude developing in a system with respect to erosion controlling parameters. Unfortunately, literature provides little such investigation; instead, it focuses more on investigating how total erosion value and erosion rate are affected by these parameters. However, two important parameters that affect erosion and raise the interest for investigation are solid particle concentration and Stokes number (check definition in Chapter 2).

Solid particle concentration is a highly associated parameter with industrial applications such as the oil and gas industry. However, limited studies have been performed on how solid particle concentration affects erosion profile, which in turn intrigues the curiosity to study such a relation. Additionally, the Stokes number is

known to characterize the nature of the behavior of solid particles in relation to the carrying fluid in a flow, which is essential to understand the corresponding development of the erosion profile. The relation between Stokes number and erosion profile has been established in literature. However, the dependency of this relation on the Stokes number's defining parameters has not been extensively reviewed, and thus it is also worth investigating.

Consequently, the main objective of this thesis is to perform a numerical parametric study on how the erosion profile of a direct jet impingement slurry flow changes in ductile material as solid particle concentration and Stokes number change. The Stokes number is studied by varying three of its defining parameters: solid particle diameter, nozzle average velocity and fluid viscosity. The idea is to evaluate if the Stokes number effect is the same on the erosion profile regardless of which of its defining parameters is changed. Additionally, the combined effect of solid particle concentration and Stokes number is investigated to check whether the erosion profile behavior remains the same under different conditions.

1.3. Research Contribution

This study develops a CFD numerical model using ANSYS CFX software to perform a parametric investigation of the effect of solid particle concentration and Stokes number on the erosion profile of a direct jet impingement slurry flow over ductile material. In addition, it investigates the possibility of the coupled effect by these two erosion controlling parameters on the profile. However, the study focuses on evaluating the Stokes number effect by varying only three of its defining parameters: solid particle diameter, nozzle average velocity and fluid viscosity.

1.4. Thesis Organization

The remainder of the thesis is organized in the following manner: Chapter 2 provides the literature survey performed to understand solid particle erosion. In addition, it describes some related work in literature to the one performed in this study. Chapter 3 discusses the methodology followed to perform the intended study. Moreover, the governing equations of implemented CFD models are presented. Chapter 4 presents the validation and parametric analysis results achieved and discusses them. Finally, Chapter 5 concludes with a summary of discovered important points and offers some ideas for future work.

Chapter 2. Background and Literature Review

In this chapter, fundamental concepts about solid particle erosion are discussed which include understanding the two different types of erosive flows, and how they are related to the Stokes number. Then, explanations of the different erosion mechanisms found in different materials, and the different controlling parameters of erosion are presented. Subsequently, the nature of erosion profile in ductile materials is explained. Following that, some different erosion modeling methods are outlined. Finally, related work in literature to the problem under analysis is discussed.

2.1. Types of Solid Particle Erosive Flows and Stokes Number

As previously mentioned, there are two types of erosive flows: slurry and dry flows. In slurry flow, the erosive solid particles are carried out by a liquid medium; whereas, in dry flow, the particles are carried out by a gas medium. The main difference between the two flows is the viscosity of each carrying medium, which determines the magnitude of entrainment the fluid has on solid particles. The higher the entrainment effect, the more the particles will follow the fluid's streamlines. One way to characterize this entrainment relation between the carrying fluid and solid particles is using the Stokes number, which is defined as the following [1,3]:

$$St = \frac{\tau_p U}{L} \tag{1}$$

$$where,\ \tau_p = \frac{\rho_p d_p^{\,2}}{18\mu_f} \tag{2}$$

where, τ_p is the particle relaxation or characteristic time, U is the fluid velocity, L is the flow characteristic length (which is the diameter of a nozzle in direct jet impingement flows), ρ_p is the particle density, d_p is the particle diameter and μ_f is the fluid dynamic viscosity.

Regardless of the fluid type, whether liquid or gas, a flow with high Stokes number indicates that the particle relaxation time is high. This in turn implements that the fluid will not be able to entrain the particles' trajectories efficiently, and thus the particles will tend to cross and not follow the fluid's streamlines. On the other hand, low Stokes number flows have a high fluid entrainment on particles motion due to the low relaxation time of the particles [1,3]. In relation to this, dry flows are usually considered high Stokes flows due to gases' relatively small viscosities whereas slurry

flows are low Stokes flows. The physical difference between the two can be better understood by looking at Fig. 1. In dry flow, the trajectories of solid particles do not follow the streamlines of the gas whereas in slurry flow, the liquid entrains solid particles, which affects their trajectories.

Consequently, dry flows are usually easier to study than slurry flows because the impacting angle of solid particles is the same as the upstream approach angle whereas in slurry flows the impacting angle has a wide range of values [1].

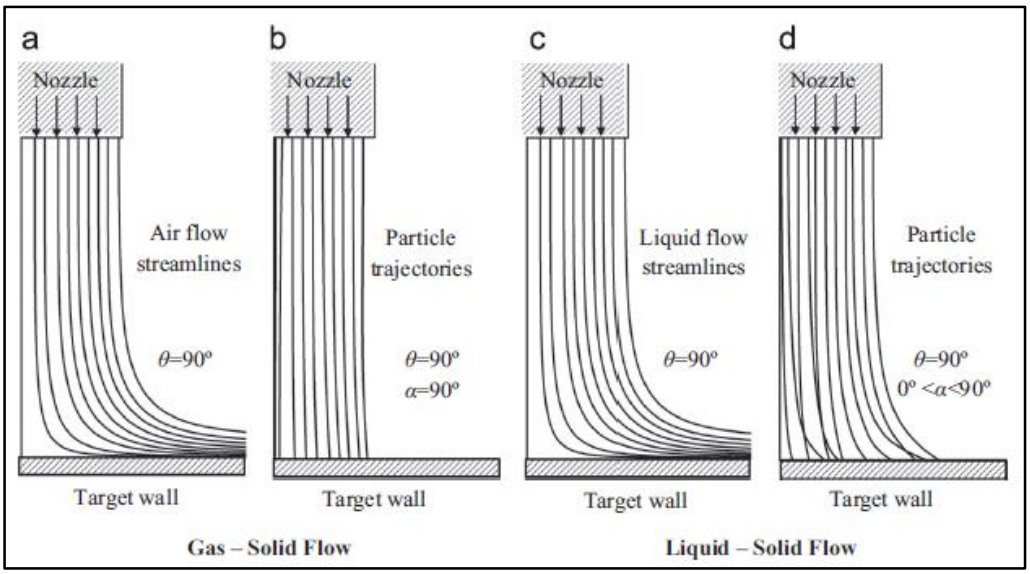

Fig. 1. The Difference in Solid Particles Trajectories between Dry and Slurry Flows: (a) and (b) Show No Change in Particle Trajectories due to Air Flow whereas (c) and (d) Show a Change in Particle Trajectories due to Liquid Flow [1].

2.2. Erosion Mechanism

It is important to understand the mechanism behind solid particle erosion; in other words, the method by which impacting particles cause erosion of the target surface. Parsi et al. [2] addressed this issue by describing different erosion mechanisms proposed by different researchers. However, they outlined that erosion mechanism differs based on the ductility of target material.

For ductile materials, there are many varying erosion mechanisms proposed by different researchers and thus there is no solid agreement on which mechanism is correct. For instance, Finnie [4] suggested a micro-geometry model to describe the erosion mechanism in ductile materials. This model states that erosion is due to micro-cutting, which is the result of a particle impacting a surface at low angle creating a crater, which is then succeeded by other particle impacts making the crater larger and

larger. However, chipped material piles up around the crater and is finally removed by successive particle impacts. On the contrary, Bellman and Levy [5] suggested a macroscopic erosion mechanism, which proposes that impacting particles cause shallow craters and platelet-like pieces on the surface of the target material. Consequently, these pieces are removed by subsequent particle impacts. Fig. 2 illustrates this mechanism.

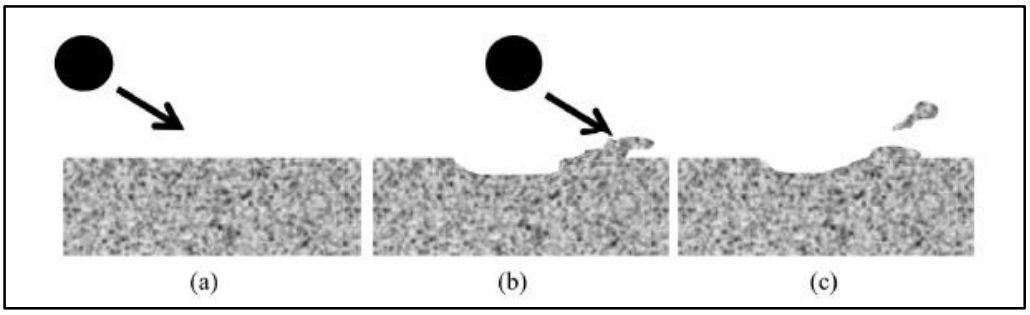

Fig. 2. Macroscopic Erosion Mechanism in Ductile Material: (a) Particle at Low Impact Angle, (b) Formation of Crater and Platelet-Like Pieces, and (c) Platelet Pieces Removal [2].

On the other hand, erosion mechanism in brittle materials is widely accepted to be due to crack formation. Impacting particles cause lateral and radial cracks, which eventually grow due to subsequent particle impacts. Consequently, these cracks cause the surface to be divided into smaller pieces which then are removed by succeeding impacting particles [2]. This can be further understood by looking at Fig. 3.

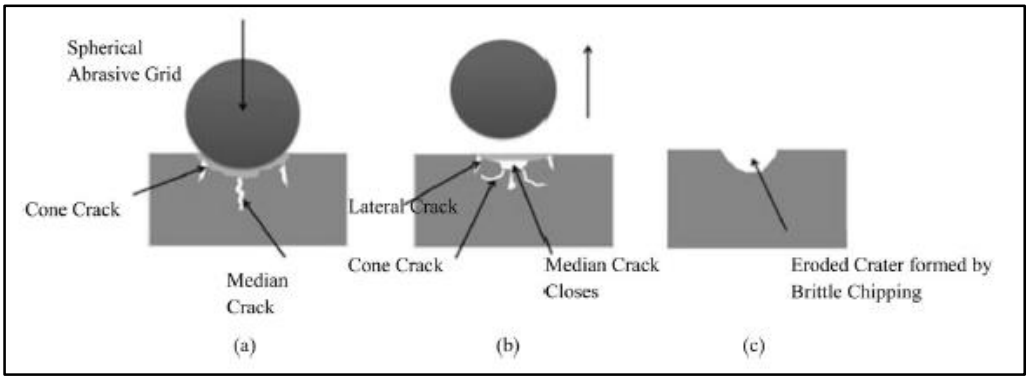

Fig. 3. Erosion Mechanism in Brittle Material: (a) Creation of Cracks, (b) Growth of Cracks and Division of Surface into Smaller Pieces, and (c) Eventual Material Removal [6].

2.3. Erosion Controlling Parameters

Solid particle erosion depends on many parameters which include: solid particle properties (shape, size and material), solid particle impact speed and angle, fluid properties, target surface properties, temperature effect and solid particle concentration [1,2]. These parameters shape the erosion models developed by researchers to predict

erosion. However, an interesting aspect to investigate is performing parametric analysis of each of these parameters to see their corresponding effect on erosion. This gives an idea of what happens to erosion when any of these parameters changes in value while other parameters remain constant. Parsi et al. [2] offered a decent review on these parametric analyses and drew conclusions about them. The following subsections outline some of these conclusions based on [2] for some parameters.

2.3.1. Particle shape. The sharper the particle is, the higher erosion it causes. Therefore, angular particles cause more erosion than spherical particles. One study that further supports this conclusion was an experiment done by Liebhard and Levy [7] in which a comparison of the effects of angular and spherical particles was performed. Consequently, it was found that the former causes greater erosion.

2.3.2. Particle size. Impacting particles with bigger sizes cause greater erosion due to their higher kinetic energy. Gandhi and Borse [8] illustrated this aspect by performing an experiment in which the effect of sand particles size on erosion of cast iron for two different impact angles (30˚ and 75˚) was performed.

Additionally, Desale et al. [9] suggested a correlation between particle size and erosion rate; see Equation 3. This correlation has been used by many researchers.

$$Erosion\ Rate \propto (Particle\ Size)^n \tag{3}$$

The value of n depends on experimental conditions, material properties, particle velocity, and particle size and size distribution. However, it ranges between 0.3 and 2.0. Consequently, based on this correlation, it can be further concluded that as particle size increases, erosion increases.

2.3.3. Particle material. The density and hardness of solid particles affect erosion. The higher the density and hardness of the particle, the greater the erosion. An experiment conducted by Levy and Chik [10] confirms this conclusion by studying the effect of solid particle hardness on erosion rate for two different impact angles (30˚ and 90˚).

2.3.4. Particle impact velocity. Erosion rate is directly proportional to the particle impact speed and both are generally related to each other by the following correlation [2]:

$$Erosion\ Rate \propto (Particle\ Impact\ Velocity)^n \quad (4)$$

where *n* is a constant defined with several different values by researchers; check [4], and [11-14]. However, Oka et al. [15], and Oka and Yoshida [16] proposed that *n* is not constant and instead depends on the hardness of target material. Despite all this, the value of *n* usually varies from 1.6 to 2.6 [2].

2.3.5. Particle impact angle. The relation between particle impact angle and erosion depends on the material of the surface under erosion. Ductile materials face higher erosion at low impact angles, and this is due to their previously described micro-cutting mechanism. On the other hand, brittle materials exhibit higher erosion at high impact angles due to their crack formation cutting mechanism. Fig. 4 shows the relation between particle impact angle and erosion rate for different brittle and ductile materials.

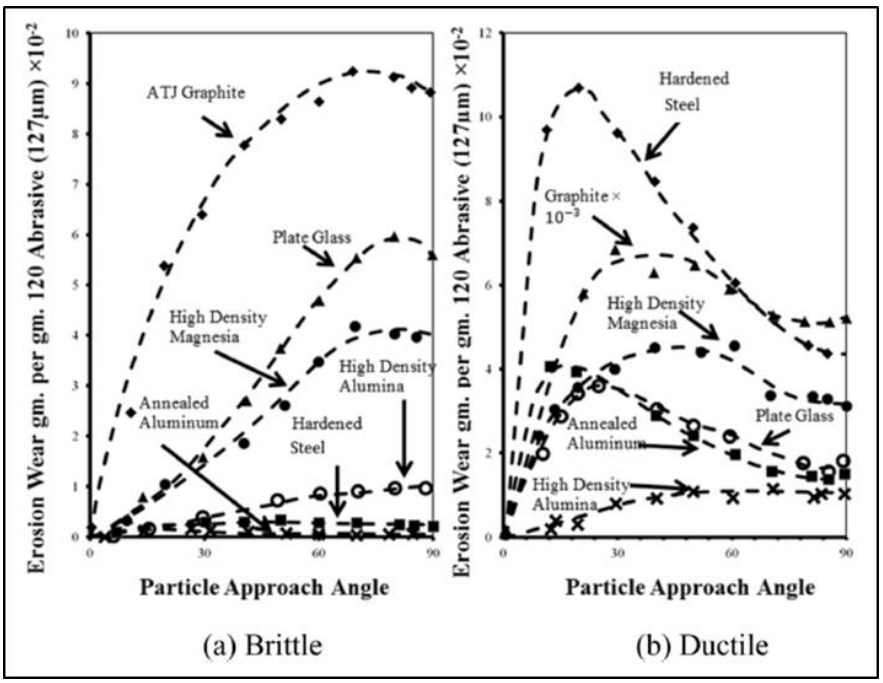

Fig. 4. Effect of Particle Impact Angle on Erosion for (a) Brittle and (b) Ductile Materials [17].

2.3.6. Particle concentration. It is generally accepted that as particle concentration increases in the flow, the erosion rate decreases. This is due to the phenomenon of "shielding" which is related to the higher particle-particle interaction that results in the flow. At high concentrations, impacting particles rebounding from the target surface tend to hit approaching particles thus reducing their speeds and correspondingly their erosion capability. Therefore, they create a shielding effect on the surface against subsequent particle impacts.

Moreover, according to Parsi et al. [2], many authors consider that this phenomenon results in decreasing the impact frequency of particles, as rebounding particles prevent others from reaching the surface, which is the real reason behind the decrease in erosion rate. However, Andrews and Horsfield [14] refute this concept by implementing that impact frequency actually does not decrease, but instead the range of impact angles of approaching particles changes due to particle-particle collision, and their impact velocities change too causing the erosion rate to decrease. They further supported their refutation by experimental and theoretical analyses.

Differently, Deng et al. [19] talk about how specific erosion rate behavior with respect to change in particle concentration is different from that of absolute erosion rate. According to [19], specific erosion rate is calculated relative to particle concentration, and tends to decrease with the increase in particle concentration due to shielding. On the other hand, absolute erosion rate keeps increasing as concentration increases. These conclusions were based on an experimental testing of the effect of particle concentration on the erosion rate of pipe bends in pneumatic conveyors.

2.4. Erosion Profile in Ductile Materials

As previously mentioned, erosion profile depends on several different parameters; two of them are material of target surface, and physics of the flow. Consequently, the surface material under investigation is of ductile type because the focus of this study is slurry flow over a ductile material. The selection of this type of material is based on its high application in industry where most of the equipment, especially in gas turbines, pumps, and oil and gas field, are made of ductile materials.

However, literature describes that erosion in ductile materials is dependent on the impact velocity and angle of solid particles [20]. Therefore, the physics of the flow is a very important parameter that dictates the shape of the erosion profile over the target surface, and this can be associated with the Stokes number. As described earlier, low Stokes flows (slurry flows) have higher entrainment of solid particles by the fluid, which in turn results in a wider range of impact angles at the surface. Therefore, in direct jet impingement flows (see Fig. 5), particles will have non-normal impact angles away from the centerline as they relatively follow the fluid's streamlines. Additionally, from Fig. 4, it can be seen that ductile materials tend to have higher erosion at low impact angles. This in turn causes the erosion profile for slurry flows in direct jet

impingement geometries to have a W-shape pattern, which correlates to maximum erosion away from the centerline as a result of the lower impact angles in that region [1,3]; check Fig. 6. On the other hand, high Stokes flows (dry flows) exhibit a U-shape erosion profile (see Fig. 6), where maximum erosion occurs at the central region. This is because particles do not follow the fluid's streamlines, and thus hit the central region and surface with normal and high impact angles. As a result, the erosion will be mainly dominated by the impact velocity effect because normal and high impact angles cause lower erosion [1,3], see Fig. 4.

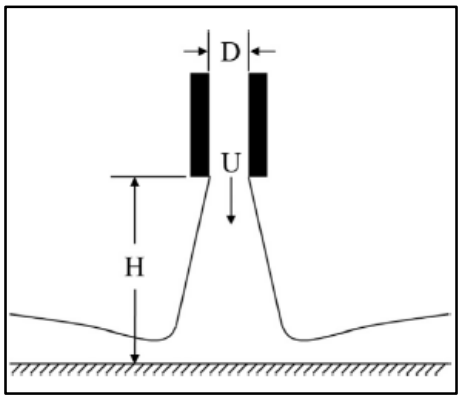

Fig. 5. Schematic of Direct Jet Impingement Geometry: *U* is Nozzle Average Velocity, *D* is Nozzle Diameter and *H* is Standoff Distance [3].

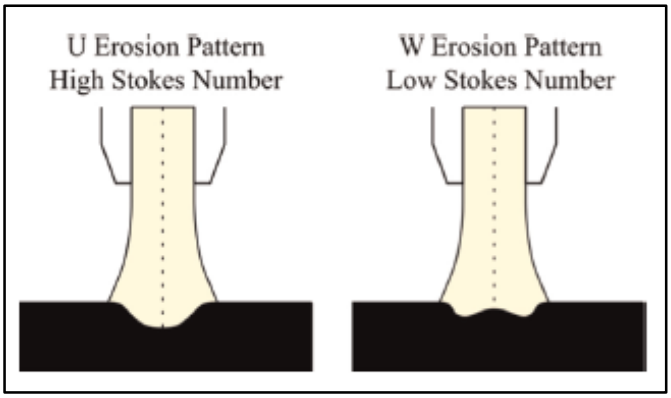

Fig. 6. Erosion Profile Shapes for High and Low Stokes Flows [3].

These erosion profile patterns in direct jet impingement setups have been observed by many studies in literature (it is important to note that this study focuses on this flow setup because it is easy to model and is widely used in literature). One such study is done by Mansouri et al. [1] in which experimental erosion profiles were measured using an optical profilometer. Erosion of steel surface was analyzed in a direct jet impingement setup where sand particles acted as the erosive particles carried by two different fluids: air (dry flow) and water (slurry flow). Two different profiles

resulted from the experiment [1]: a U-shape erosion profile, which is associated with the dry flow, and a W-shape erosion profile corresponding to the slurry flow. Additionally, several other studies have also identified the W-shape profile for slurry flows over ductile materials in direct jet impingement setups; see [21] and [22].

However, it is worth clarifying that these shapes are corresponding to the value of the Stokes number rather than the type of carrying fluid. In other words, if a slurry flow has high Stokes number, it can exhibit the erosion profile shape of a dry flow i.e. U-shape. This in fact was demonstrated by Giourntas et al. [23] in which a slurry flow with high Stokes number resulted with an erosion profile similar to that of dry flow. In relation, this thesis studies the Stokes number effect on the erosion profile while maintaining the liquidity of the carrying fluid. In other words, the Stokes number is investigated for a slurry flow. The reason behind the selection of slurry over dry flow for analysis is that it is more common in industrial applications such as pipelines, pumps, fluidized beds, online wash systems of gas turbines, oil and gas field, and others.

2.5. Erosion Modeling

Solid particle erosion prediction depends on developing models that could calculate erosion in systems so that it can be avoided or treated. Consequently, there are many erosion modeling techniques available in literature, and thus this section aims at listing and describing some of them. However, it is important to clarify that the erosion models listed in this section describe general erosion of surfaces by impacting solid particles. In other words, the geometry of the flow is general, not belonging to a specific setup such as inline of pipes, T-junctions, valves, direct jet impingement and others.

First, the most fundamental and earliest proposed solid particle erosion model was proposed by Finnie [20]. The author explained that surface erosion depends on abrasive particle motion and material properties of both the particle and eroding surface. Finnie [20] proposed two equations for calculating volume of surface material removed by a single abrasive particle for low and high impact angles. The author's model depends on the assumptions that a) "the ratio of the depth of contact to the depth of cut is constant", b) "the width of particle cutting face is uniform and is large compared to the depth of cut", and "c) constant plastic flow is reached upon impact of particles" [2]. However, this model fails to predict any erosion when the impact angle is normal to the

surface. Finnie [20] also states that, based on experimental work, this model works fine to predict erosion caused by many particles for low impact angle. The model is as follows:

$$\varepsilon_{VP} = \frac{m_p V_p^2}{P\psi\kappa}\left(\sin(2\alpha) - \frac{6}{\kappa}\sin^2(\alpha)\right) \; for \tan\alpha \le \frac{\kappa}{6} \tag{5}$$

$$\varepsilon_{VP} = \frac{m_p V_p^2}{P\psi\kappa}\left(\frac{\kappa\cos^2\alpha}{6}\right) \; for \tan\alpha \ge \frac{\kappa}{6} \tag{6}$$

Another erosion model was proposed by Bitter [24,25] in which erosion is considered to be caused by two mechanisms: repeated deformation and cutting. The author's first model described erosion caused due to repeated deformation mechanism and was based on energy balance for plastic-elastic collision. However, Bitter [24] reported that this model proves to predict well erosion behavior of brittle materials for different impact angles as compared with experimental data. The model is as the following:

$$\varepsilon_{VP} = \frac{1}{2}\frac{M\left(V_p\sin\alpha - K\right)^2}{\delta} \tag{7}$$

Bitter's [25] second model described erosion caused by cutting mechanism and depends on whether or not impacting particles have horizontal velocity component when leaving the target surface. This model has two criteria as the following:

$$\varepsilon_{VC1} = \frac{2MV_p\left(V_p\sin\alpha - K\right)^2}{(V_p\sin\alpha)^{1/2}}\left[V_p\cos\alpha - \frac{C(V_p\sin\alpha - K)^2}{(V_p\sin\alpha)^{1/2}}\chi\right] \; for \; \alpha \ge \alpha_{p0} \tag{8}$$

$$\varepsilon_{VC2} = \frac{\frac{1}{2}M\left[V_p{}^2\cos^2\alpha - K_1(V_p\sin\alpha - K)^{3/2}\right]}{\chi} \; for \; \alpha \le \alpha_{p0} \tag{9}$$

Consequently, the total erosion accordingly is the sum of erosion caused by these two mechanisms and can be described as the following:

$$\varepsilon_{VT} = \varepsilon_{VP} + \varepsilon_{VC} \tag{10}$$

Based on the work of Finnie [20], and Bitter [24,25], Neilson and Gilchrist [8] proposed a new model which considers erosion as caused by both cutting and deformation mechanisms. They explained that the parallel component of kinetic energy of impacting particles is responsible for cutting erosion whereas the normal component

causes deformation erosion. However, their study implies that further analysis is needed to define cutting and deformation wear factors. Their erosion model is described as the following and takes into consideration erosion caused by small and large impact angles:

$$\varepsilon_V = \frac{\frac{1}{2}M\left(V_p{}^2\cos^2\alpha - V_r{}^2\right)}{\chi} + \frac{1}{2}\frac{M(V_p\sin\alpha - K)^2}{\delta} \quad for\ \alpha < \alpha_{p0} \tag{11}$$

$$\varepsilon_V = \frac{\frac{1}{2}MV_p{}^2\cos^2\alpha}{\chi} + \frac{1}{2}\frac{M(V_p\sin\alpha - K)^2}{\delta} \quad for\ \alpha > \alpha_{p0} \tag{12}$$

However, Finnie [26] came up with a modified erosion model over the author's previous one, which has better prediction of erosion in ductile metals. The following erosion rate predicting model is proposed by Finnie [26]:

$$\begin{aligned} \varepsilon_V &= \frac{cMV_p{}^2}{4P(1+m_p r^2/I)}\left(\cos^2\alpha - \frac{\dot{x}_t'}{V_p}\right) \\ where, &\begin{cases} \dot{x}_t' = V_p\cos\alpha - \dfrac{2V_p}{P}\sin\alpha \end{cases} \end{aligned} \tag{13}$$

Finnie [26] further simplified the previous model in case the cutting mechanism in erosion stops which is either the case when there is no horizontal component of particle tip velocity or the particle is not touching the surface while its tip is moving horizontally. However, this model suffers low accuracy when the impact angle is close to 90º. The simplified model is described as the following:

$$\varepsilon_V = \frac{cMV_p{}^2}{4P(1+m_p r^2/I)}\cos^2\alpha \quad for\ \dot{x}_t' = 0 \tag{14}$$

$$\varepsilon_V = \frac{cMV_p{}^2}{4P(1+m_p r^2/I)}\left(\sin(2\alpha) - \frac{2\sin^2\alpha}{P}\right) \quad for\ y_t = 0 \tag{15}$$

On the other hand, an empirical based model was proposed by Sheldon and Kanhere [27] which depends on indentation hardness characteristics of materials for single particles. However, this model is valid only for erosion at a normal impact angle and low impact velocities. This model predicts total loss of volume as the following:

$$\varepsilon_{VT} = \frac{d_p{}^3V_p{}^3\rho_p{}^{3/2}}{H_V{}^{3/2}} \tag{16}$$

In a different approach to model erosion of ductile materials, Tilly [28] proposed a two-stage mechanism for erosion. The primary stage is responsible for erosion due to particles impacting the surface and chipping off material. The secondary stage causes erosion by impacting particles breaking up into fragments around the scar created by the primary stage; however, the secondary stage is only available when impacting particles break up. Consequently, the total erosion rate is the sum of erosion rates by primary and secondary stages and is described as the following:

$$\varepsilon_V = \widehat{\varepsilon}_1 \left(\frac{V_p}{V_{ref}} \right)^2 \left[1 - \left(\frac{d_0}{d_p} \right)^{3/2} \left(\frac{V_0}{V_{ref}} \right) \right]^2 + \widehat{\varepsilon}_2 \left(\frac{V_p}{V_{ref}} \right)^2 F_{d,V}$$
$$where, \begin{cases} F_{d,V} = \dfrac{W_0 - W}{W_0} \end{cases} \tag{17}$$

However, Jennings et al. [29] explained and experimentally showed that a major mechanism of erosion in ductile materials is the melting of the eroding target surface. Consequently, they developed a mathematical model based on dimensional analysis to predict erosion rate as the following:

$$\varepsilon_V = \frac{{K_T}^{5/2}}{R} \left(\frac{G^{1/3}}{{\rho_t}^{1/3} k T_m \Delta H_m} \right) \tag{18}$$

In an experimental effort, Hutchings et al. [30] proposed a simple correlation to calculate erosion rate based on experimental results. In their study, erosion experiments of spherical steel particles impacting mild steel were performed, and it was revealed that results of these experiments closely mimic erosion of sand particles on metals. According to this correlation, erosion rate is calculated as the following:

$$\varepsilon_m = 5.82 \times 10^{-10} {V_p}^{2.9} \tag{19}$$

Hutchings [31] also developed a mechanistic model to calculate the erosion rate of metals eroded by spherically shaped particles at a normal impact angle. This model assumes that impacting particles do not fracture or deform, and neglect elastic effects. However, despite the inclusion of ductility and dynamic hardness in the model, more analysis is required to determine their values and utilize them in the model; described as the following:

$$\varepsilon_m = 0.033 \frac{\alpha \rho_t P^{0.5} V_p{}^3}{\Omega_c{}^2 H_t{}^{1.5}} \tag{20}$$

Another model was proposed by Evans et al. [32] which takes into consideration erosion of brittle materials in the elastic-plastic response regime. The proposed model describes a relation between formation of radial crack and fracture toughness of target surface, and is as the following:

$$\varepsilon_{VP} \propto \frac{V_p{}^{19/6} r^{11/3} \rho_p{}^{1/4}}{K_c{}^{4/3} H_t{}^{1/4}} \tag{21}$$

A very interesting and well-rounded semi-empirical model was proposed by Tabakoff et al. [33] and is applicable to all ranges of impact angles (small, intermediate, large and a combination of all). This model is characterized by taking into consideration the particle tangential restitution coefficient and is as the following:

$$\varepsilon_m = K_1 f(\alpha) V_p{}^2 \left(\cos^2 \alpha\right)\left(1 - e_t{}^2\right) + f(V_p, n)$$

$$where, \begin{cases} e_t = 1 - 0.0016 V_p \sin\alpha \\ f(\alpha) = \left\{1 + K_4 K_2 \sin\left(\frac{\pi}{2} \frac{\alpha}{\alpha_m}\right)\right\}^2 \\ f(V_p, n) = K_3 \left(V_p \sin\alpha\right)^4 \\ K_4 = \begin{cases} 1, & \alpha \le 3\alpha_m \\ 0, & \alpha > 3\alpha_m \end{cases} \end{cases} \tag{22}$$

An analytical erosion model was proposed by Sundararajan and Shewmon [34] which takes into consideration a localization concept approach. This means that at a certain strain, called critical strain, plastic deformation on target surface localizes forming a lip of material, which in turn is removed causing erosion. This model assumes that plastic deforming volume and crater volume are proportional. Several versions of the proposed erosion model were described in the study; however, a simplified form was defined as the following:

$$\varepsilon_m \approx \frac{6.5 \times 10^{-3} V_p{}^{2.5} \rho_p{}^{2.5}}{C_p T_m{}^{0.75} H_t{}^{0.25}} \tag{23}$$

Furthermore, Sundararajan [35] proposed two erosion models to calculate erosion rate caused by normal and oblique impact angles. The author then combined both to come up with an overall model for erosion of ductile materials for all particle impact angles and different shapes. The basis of this model is the previously explained

localization of plastic deformation concept. The comprehensive model is as the following:

$$\varepsilon_m = \left(\frac{2^{n_h} C V_p^{\,2} \left(\sin^2 \alpha\right) F(t)}{n_h C_p} \right) \left[1 + \left\{ \frac{\left(n_h + 1\right)\left(\frac{\mu}{\mu_c} \right)\left(2 - \frac{\mu}{\mu_c} \right)}{4\left(1+\lambda\right)\left(\tan^2 \alpha\right) F(t)} \right\} - e^2 \right] \qquad (24)$$

$$where, \begin{cases} e = \dfrac{1.9 H_p^{\,5/8}}{E_e^{\,1/2} \rho_p^{\,1/8} V_p^{\,1/4}} \\ F(t) \approx 0.02 - 0.05 \end{cases}$$

Venougopal Reddy and Sundararajan [36] conducted a set of experiments of erosion on two ductile materials using a constant velocity of 40 m/s and three impact angles (30º, 60º and 90º). Surprisingly, they found that maximum erosion is at normal impact angle which contradicts the general understanding of solid particle erosion of ductile materials. Additionally, they proposed the following model to calculate erosion rate based on the localization concept previously explained:

$$\varepsilon_{VP} \propto \frac{L^3 \Delta\Omega_m}{\Omega_C} \qquad (25)$$

A statistical model was developed by Johansson et al. [37] to calculate erosion rate of brittle single-crystal materials. It was found that erosion is mainly caused by brittle fracture. The proposed model is as the following:

$$\varepsilon_m = (1-f) K_1 \frac{\rho_t \rho_p^{\,2/9} E_t^{\,2/3} V_p^{\,22/9} d_p^{\,2/3}}{H_t^{\,5/9} K_c^{\,4/3}} + f K_2 \frac{\rho_t \rho_p^{\,1/3} E_t V_p^{\,8/3} d_p}{H_t^{\,1/3} K_c^{\,2}} \qquad (26)$$

An empirical approach was performed by Ahlert [38] to determine the erosion rate for direct impingement of carbon steel with wet and dry surfaces for different impact angles and particle shapes. The model is as the following (the particle impact angle function, $F(\alpha)$, was defined by Zhang et al. [39], and the values of *Ai* and *Fs* were determined experimentally):

$$\varepsilon_m = 2.17 \times 10^{-7} \times (BH)^{-0.59} F_s V_p^{\,2.41} F(\alpha)$$
$$where, \begin{cases} F(\alpha) = \sum_{i=1}^{5} A_i \alpha^i \end{cases} \qquad (27)$$

Oka et al. [15] developed on the previous model by Ahlert [38] to take into account the effect of target material hardness, particle properties and particle diameter on erosion prediction. Consequently, they proposed the following model:

$$\varepsilon_V(\alpha) = f(\alpha)\varepsilon_{90}$$
$$where, \begin{cases} \varepsilon_{90} = K_p (H_V)^{k_1} (V_p)^{k_2} \left(d_p \times 10^{-6}\right)^{k_3} \\ f(\alpha) = (\sin\alpha)^{n_1} \left(1 + H_V (1 - \sin\alpha)\right)^{n_2} \end{cases} \quad (28)$$

However, Levin et al. [40] proposed that to accurately model the erosion mechanism, the effect of mechanical properties of the eroding particles and target surface in addition to the work hardening effect produced during the erosion process should be accounted for. Consequently, they generated the following erosion model for ductile alloys:

$$\varepsilon_m = \frac{m_p V_p^{\,2}}{2} \left[\frac{1 - \left(\frac{3.06 H_t^{\,5/4}}{\rho_p V_p^{\,1/2}} \right) \left(\frac{1-\mu_t^{\,2}}{E_t} + \frac{1-\mu_p^{\,2}}{E_p} \right)}{TL_v} \right] \quad (29)$$

Furthermore, Mansouri et al. [1] performed a combined experimental and CFD study to generate their own erosion prediction model for direct jet impingement flow. However, they based their approach on an erosion model developed by a combination of studies by [20,39,41], which is a widely accepted model for prediction of erosion in metals. The model developed by Mansouri et al. [1] can be expressed as the following:

$$\varepsilon_m = a F_s V_p^{\,n} f(\alpha) \;\; where, \;\; f(\alpha) = a_1 \times (\sin\alpha)^{b_1} \times (1.5 - \sin\alpha)^{b_2} \quad (30)$$

This model implies that erosion is a function of material properties of particles and target surface, particle impact angle and particle impact speed. By combining numerical and experimental results, Mansouri et al. [1] were able to define the particle impact angle function as shown in the model.

2.6. Related Work

As mentioned earlier, this study aims at performing numerical parametric analysis of erosion profile for direct jet impingement slurry flow over ductile target surface. The erosion controlling parameters considered for this study are the solid particle concentration and Stokes number. Consequently, there are many experimental

and numerical erosion studies in literature with similar flow setups and target material (check [1,21-23,42-46]). A brief description of some of these studies is as the following:

- Wang et al. [21] numerically and experimentally studied the effect of solid particle concentration and nozzle velocity on the total weight loss of two target materials: stainless steel 304 and 44W carbon steel. The flow studied was of slurry type of water carrying sand particles in direct jet impingement setup for two cases: submerged and non-submerged setups.

- Turenne et al. [22] experimentally evaluated how the erosion rate changes with solid particle concentration. Two target materials (aluminum and glass) were eroded by sand particles carried by a water fluid medium in a direct jet impingement geometry.

- Mansouri et al. [42] numerically and experimentally investigated how erosion ratio and erosion profile change with different fluid viscosity and solid particle diameter at low solid particle concentration. The analysis was carried out for slurry flow of water carrying sand particles over stainless steel 316 target surface in a direct jet impingement setup.

- Nguyen et al. [43] numerically and experimentally studied the effect of nozzle velocity on erosion rate of stainless steel SUS304 by water carrying sand particles. The flow geometry was of a direct jet impingement type.

- Li et al. [44] experimentally looked at the change in total erosion with respect to change in solid particle concentration and nozzle velocity. Three different target materials were investigated: copper, aluminum and mild steel. Moreover, three different slurry flows were used: coal particles carried by kerosene, Al_2O_3 particles carried by water, and SiC carried by water. All the tests were performed in a direct jet impingement setup.

- Mansouri et al. [45] numerically and experimentally investigated the effect of solid particle concentration and fluid viscosity on the erosion rate of stainless steel 316 by water carrying sand particles. Direct jet impingement flow geometry was utilized in the study.

By considering the previous description and literature, it can be seen that there is a huge focus by researchers on how the erosion rate and total erosion change with respect to change in erosion controlling parameters such as solid particle concentration

and Stokes number (by changing its defining parameters in Equations 1 and 2). However, little interest in the change of erosion profile as result of change in the controlling parameters has been covered by literature except; for Frosell et al. [3] and Mansouri et al. [42]. Consequently, this thesis aims at tackling this aspect in addition to investigating the combined effect of solid particle concentration and Stokes number, which also has been little investigated before. Furthermore, the current study attempts to test how changing different defining parameters in Stokes number affects the erosion profile.

Chapter 3. Methodology

The aim of this study is to perform numerical parametric analysis of the erosion profile for direct jet impingement slurry flow over ductile material. Consequently, the numerical analysis was performed using ANSYS CFX software as it is an available finite element CFD tool. The software follows a specific series of steps in defining a fluid flow problem and solving it: first, the geometry of the flow is created and meshed (i.e. divided into small finite elements), second, the boundary conditions are defined and the flow is solved, finally, the solution is post processed to obtain the needed results. Usually erosion problems are studied experimentally due to their sensitivity, and many erosion controlling parameters are determined empirically; therefore, theoretical methods are not very efficient in erosion studies. However, experimental methods suffer from high costs, experimental errors, environmental dependency, reliance on high sensitivity measuring tools, and many other difficulties. On the other hand, CFD methods have no experimental errors, give access to many valuable parameters and quantities, provide 3D results with ease, allow more insight into the problem, require less cost to perform, give flexibility in parametric analysis, and allow repeatability of results. Therefore, CFD method was selected to perform the intended parametric study.

Thus, this chapter provides an overall description of the flow under analysis, lists the different flow governing equations implemented in CFD, and describes the different parts of the developed CFD model.

3.1. Overview of Flow under Analysis

3.1.1. Specifications of basic flow. The work done by Mansouri et al. [1] was considered as the basis for this study so that the developed CFD model can be better validated. Consequently, the specifications of the basic flow under analysis (i.e. before performing parametric study) were derived from [1] and are as the following:

- Slurry flow of water carrying sand particles
- Direct jet impingement setup as in Fig. 5
- Impingement angle: 90º; i.e., the nozzle is normal to the target (coupon) surface
- Nozzle diameter: 7mm

- Stand-off distance (distance between nozzle and coupon): 12.7mm
- Nozzle average velocity (U): 14m/s
- Coupon material: Stainless steel 316
- Sand particle diameter (d_p): 300microns
- Sand particle shape: Spherical
- Sand particle density: 2650kg/m^3
- Sand particle concentration by weight: 1%
- Test duration: 6h

Additionally, the flow was simulated in CFD as steady isothermal flow which is a common practice in literature to simplify calculation cost; check [1,21,42,43,45,46]. Moreover, water's dynamic viscosity (μ_f) was taken to be 0.8899cp.

3.1.2. Specifications of flow under parametric study. As mentioned earlier, a parametric study is performed in this thesis by varying the solid particle concentration (C_w or C_v) and Stokes number (St). However, the latter was altered by changing three of its defining parameters (d_p, U *and* μ_f); this was done to investigate if the effect on the erosion profile changes with respect to different parameters in the Stokes number.

The tested range of particle concentration was based on reviewing the literature (see [3]) to determine what constitutes low and high values. Additionally, three Stokes numbers were taken into consideration such that they differ by one order of magnitude to ensure the significant difference between them, and thus enables the possibility to notice any differences in their effects on the erosion profile. Furthermore, each Stokes number was also evaluated at two extreme particle concentrations (low and high) to investigate the coupled effect. Table 1 and 2 show the associated values considered in the parametric study (the default values corresponding to the basic flow specifications by [1] are italicized).

Table 1: Concentration Values (by Weight and Volume) for Parametric Study.

C_w	*1%*	8%	15%	22%
C_v	*0.38%*	3.18%	6.24%	9.62%

Table 2: Stokes Number Values for Parameteric Study.

St	2.98	*29.8*	298
d_p **(microns)**	94.9	*300*	949
U **(m/s)**	1.4	*14*	140
μ_f **(cp)**	8.893	*0.8899*	0.08893

3.2. Governing Equations

The flow under analysis is multiphase consisting of liquid water and sand particles. Consequently, ANSYS CFX models this flow using the Eulerian-Lagrangian approach in which water is treated as a continuous medium and modeled with an Eulerian method. On the other hand, sand particles are considered a discrete phase in which they are tracked through the flow in a Lagrangian fashion [47]. The continuous phase is governed by the Reynolds averaged continuity and Navier-Stokes equations. Additionally, the SST (Shear Stress Transport) turbulence model was selected to calculate the fluid flow and maintain the similarity, for validation purpose, with the numerical method by Mansouri et al. [1]. Furthermore, the discrete phase is governed by its equation of motion. However, the particle effect on water (two-way coupling) and particle-particle collision (four-way coupling) were also considered in this study. The erosion caused by sand particles is modeled in CFX using the built-in Finnie model; check [48-50]. A description of these governing equations is outlined in this section.

3.2.1. Continuous phase. Since the flow is isothermal, this phase is governed by the Reynolds averaged continuity and Navier-Stokes equations without taking into consideration the energy equation. Consequently, the equations are as the following (respectively) [47]:

$$\frac{\partial \rho}{\partial t} + \frac{\partial}{\partial x_j}\left(\rho U_j\right) = 0 \tag{31}$$

$$\frac{\partial \rho U_i}{\partial t} + \frac{\partial}{\partial x_j}\left(\rho U_i U_j\right) = -\frac{\partial p}{\partial x_i} + \frac{\partial}{\partial x_j}(\tau_{ij} - \rho\overline{u_i u_j}) + S_M \tag{32}$$

where, $\rho\overline{u_i u_j}$ is the Reynolds stress term which can be defined based on the eddy viscosity model as [47]:

$$-\rho\overline{u_i u_j} = \mu_t\left(\frac{\partial U_i}{\partial x_j} + \frac{\partial U_j}{\partial x_i}\right) - \frac{2}{3}\delta_{ij}\left(\rho k + \mu_t \frac{\partial U_k}{\partial x_k}\right) \tag{33}$$

where, k is the turbulent kinetic energy, and μ_t is the turbulent viscosity and its definition resembles the turbulence model used. Since the SST turbulence model is considered, μ_t is defined as the following [47]:

$$\mu_t = \rho\frac{k}{\omega} \tag{34}$$

where, ω is the turbulent frequency. Thus, the SST model equations are defined as [47]:

$$\frac{\partial(\rho k)}{\partial t} + \frac{\partial}{\partial x_j}\left(\rho U_j k\right) = \frac{\partial}{\partial x_j}\left[\left(\mu + \frac{\mu_t}{\sigma_{k3}}\right)\frac{\partial k}{\partial x_j}\right] + P_k - \beta'\rho k\omega + P_{kb} \tag{35}$$

$$\frac{\partial(\rho\omega)}{\partial t} + \frac{\partial}{\partial x_j}\left(\rho U_j \omega\right) = \frac{\partial}{\partial x_j}\left[\left(\mu + \frac{\mu_t}{\sigma_{\omega 3}}\right)\frac{\partial \omega}{\partial x_j}\right] + (1-F_1)2\rho\frac{1}{\sigma_{\omega 2}\omega}\frac{\partial k}{\partial x_j}\frac{\partial \omega}{\partial x_j} + \alpha_3\frac{\omega}{k}P_k - \beta_3\rho\omega^2 + P_{\omega b} \tag{36}$$

where, F_1 is a blending function (for definition see [47]), P_{kb} and $P_{\omega b}$ represent the influence of buoyancy forces (for definition see [47]), P_k is the turbulence production due to viscous forces (for definition see [47]), and α_3, β', β_3, σ_{k3}, $\sigma_{\omega 2}$ and $\sigma_{\omega 3}$ are constants.

3.2.2. Discrete phase: One-way coupling. If the particles' effect on the fluid is not taken into account, the flow analysis is considered one-way coupled. This is a common approach in literature for low particle concentration slurry flows; see [1,21,42,43,45,46]. Consequently, the particles are tracked in the continuous medium

and the forces acting on them determine their motion. These forces are governed by the following equation of motion [47]:

$$m_p \frac{dU_p}{dt} = F_D + F_B + F_R + F_{VM} + F_P + F_{BA} \tag{37}$$

where, U_p is the particle velocity, F_D is the drag force, F_B is the buoyancy force, F_R is the forces due to domain rotation, F_{VM} is the added mass force, F_P is the pressure gradient force, and F_{BA} is the Basset force. However, this study considers the drag force to be dominant and thus Equation 37 simplifies to:

$$m_p \frac{dU_p}{dt} = F_D \tag{38}$$

where, F_D is defined as the following [47]:

$$F_D = \frac{1}{2} C_D \rho_f A_f |U_S| U_S \tag{39}$$

where, C_D is the drag coefficient, ρ_f is the fluid density, A_f is the effective particle cross section, and U_S is the slip velocity between the fluid and particle. The drag coefficient is calculated using the Schiller Naumann drag model which is as the following [47]:

$$C_D = \max\left(\frac{24}{\mathrm{Re}_p}\left(1 + 0.15\,\mathrm{Re}_p^{\,0.687}\right), 0.44 \right) \tag{40}$$

where, Re_p is the particle Reynolds number defined as [21]:

$$\mathrm{Re}_p = \frac{\rho_f |U_R| d_p}{\mu_f} \tag{41}$$

where, U_R is the relative velocity between the particle and fluid.

3.2.3. Discrete phase: Two-way coupling. When the effect of particles motion on fluid behavior is taken into account, the flow analysis is described as two-way coupled. Consequently, to model two-way coupling, particle momentum source terms, generated from forces, need to be included in the fluid momentum equations [47]. In relation, the particle momentum source corresponding to drag force is modeled as the following [47]:

$$\frac{dS}{dt} = -F_D = -\frac{1}{2} C_D \rho_f A_f |U_S| U_S \tag{42}$$

where, *S* is the source term added to the continuous momentum equation.

3.2.4. Particle-particle collision: Four-way coupling. ANSYS CFX provides a particle-particle collision model, which takes into account interaction of particles and their effects on both discrete and continuous phases; hence referred to as four-way coupling. It is a stochastic model that expands the Euler-Lagrange model to include particle-particle collision by introducing the concept of virtual collision partner to the real particle (for more information check [47]). The set of governing equations of the model is as the following [47]:

$$\begin{cases} v'_{2,i} = R(St_t)v'_{1,i} + \sigma_{P,i}\sqrt{1-R(St_t)^2}\,\xi \\ f_c = \dfrac{\pi}{4}(d_{p1}+d_{p2})^2\left|\vec{v_1}-\vec{v_2}\right|n_P \\ P_c = 1-\exp(-f_c\Delta t) \end{cases} \tag{43}$$

where, indices 1 and 2 stand for real and virtual particles respectively, index *i* indicates the three coordinate directions, prime represents the fluctuating component of velocity, $\sigma_{P,i}$ is the *i*-th component of mean fluctuating velocity in numerical control volume, ξ is a Gaussian random number, f_c is the collision frequency, P_c is the collision probability, $\vec{v_1}$ and $\vec{v_2}$ are the instantaneous velocities of real and virtual particles respectively, Δt is the numerical time step, and $R(St_t)$ is the Sommerfeld's correlation function defined as the following [47]:

$$R(St_t) = \exp(-0.55St_t^{0.4}) \tag{44}$$

where, St_t is the turbulent Stokes number defined as the following [47]:

$$St_t = \frac{\rho_p d_p^{\,2}\varepsilon}{0.3(18)\mu_f k} \tag{45}$$

Also, n_P in Equation 43 is the particle number density and is defined as [47]:

$$n_P = \frac{\sum \dot{N}\Delta t}{Vol_{CV}} \tag{46}$$

where, $\dot{N}$ is the particle number rate and Vol_{CV} is the volume of numerical control volume.

3.2.5. Erosion model. The erosion model implemented in this study was ANSYS CFX's built-in Finnie model, which is based on works by [49,50]. This model was selected because it is already coded into the software, and thus eliminates the need to be personally implemented. However, CFX further adjust the model and thus becomes defined as the following [48]:

$$E = \left(\frac{V_p}{V_0}\right)^n f(\gamma) \tag{47}$$

where, n is an empirical constant taken by this study to be 2.4 as done by Mansouri et al. [1], V_0 is the reference velocity having different values based on different target materials (see Table 3), and $f(\gamma)$ is the function of impact angle and is defined as [49]:

$$\begin{cases} f(\gamma) = \frac{1}{3}\cos^2\gamma & if\ \tan\gamma > \frac{1}{3} \\ f(\gamma) = \sin(2\gamma) - 3\sin^2\gamma & if\ \tan\gamma \le \frac{1}{3} \end{cases} \tag{48}$$

Table 3: Values for V_0 in Equation 47 [48].

V_0(m/s)	Target Material
952	Aluminum
661	Copper
1310	Mild Steel
3321	Hardened Steel

Values of V_0 in this study were taken to be 2100m/s for the one-way and two-way coupling simulations, and 2300m/s for the four-way coupling simulations. The selection of these values was based on trial and error effort to achieve results close to that by Mansouri et al. [1] due to the lack of needed data to know the exact value of V_0. However, it can be noticed that the two selected values are between those of mild and hardened steels (Table 3), which confirms the selection because the coupon material under analysis is stainless steel 316.

3.3. CFD Setup

3.3.1. Geometry of flow domain. The geometry of the developed CFD model was based on a direct jet impingement setup similar to that in Fig. 5 and by Mansouri et al. [1]. It consists of a nozzle spraying water carrying sand particles onto a coupon (or target surface). However, the coupon was not geometrically modeled; instead, it was taken as a wall boundary condition onto which the erosion model is applied (Equations 47 and 48). Fig. 7 shows the developed geometric model of the flow. As can be seen, there is a small box inside the flow: this was done to implement multizone meshing technique, and is explained in the following subsection.

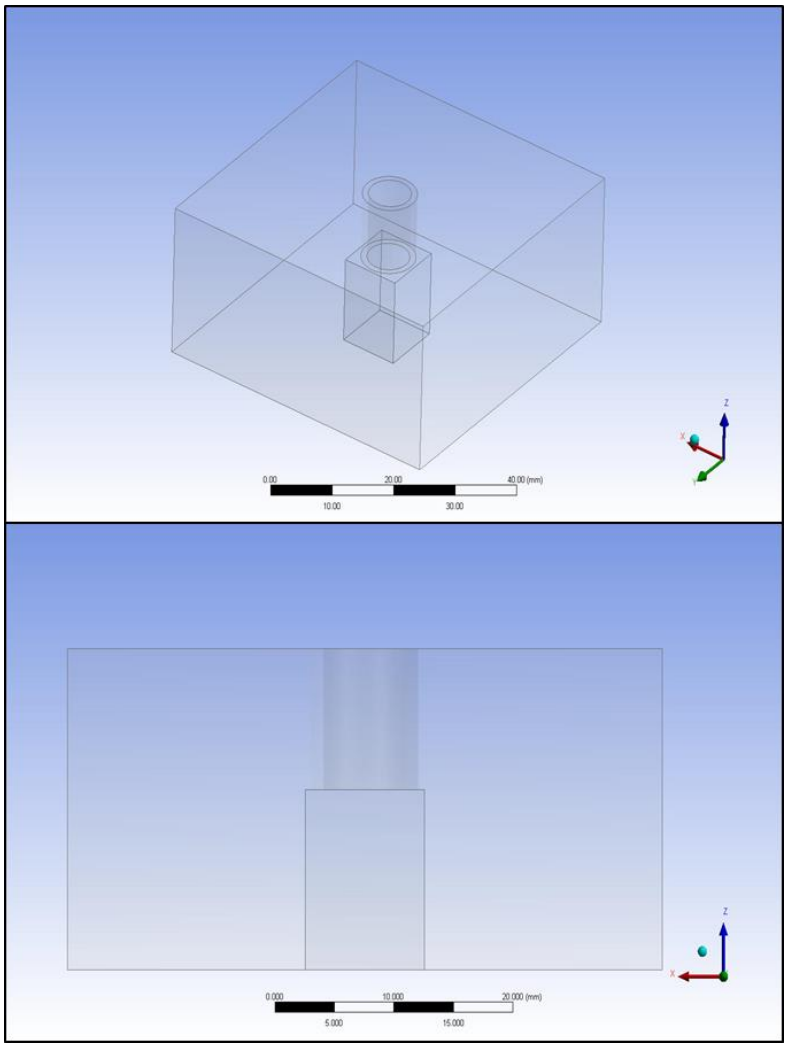

Fig. 7. Geometry of Flow Domain

3.3.2. Meshing. Since the analysis is numerical, dividing the geometry into small finite elements and nodes is important to solve the numerical problem. This is referred to as meshing. As seen in Fig. 8, hexahedral element type was selected to mesh the domain with the implementation of different element sizes at three different regions:

nozzle, refined box and surrounding flow. The concept is to refine the mesh size in regions of high interest, corresponding to the nozzle interior and the jet spread area over the coupon where most of the erosion occurs. In Chapter 4, results from three different mesh sizes were compared to select the mesh independent setup in which the solution is independent of the mesh size.

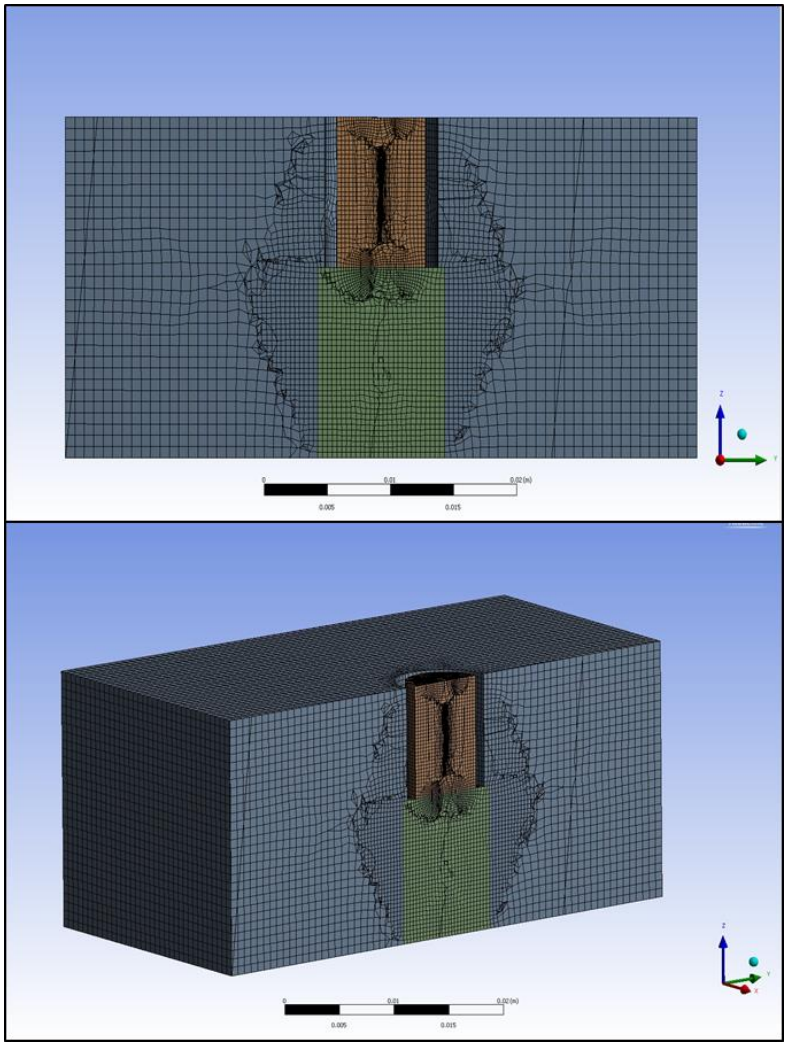

Fig. 8. Cross Section of Multizone Mesh

3.3.3. Boundary conditions. This is a very critical step in numerical solving where the boundary conditions are imposed on the problem, and thus dictating the solution. The selected boundary conditions by this study were as the following:

- Nozzle inlet: A fully developed turbulent velocity profile following the one seventh power law was implemented to ensure that the fluid velocity profile exiting the nozzle is fully developed; indicated with black arrows in Fig. 9.

- Coupon: A no-slip wall boundary condition was used on which the Finnie erosion model is calculated (Equations 47 and 48).
- Nozzle walls: A no-slip wall boundary condition was utilized.
- Surrounding flow surfaces: An opening boundary condition was implemented to allow the flow to exit the flow domain; indicated with blue arrows in Fig. 9.
- Water-Sand coupling: One-way, two-way and four-way (i.e. particle-particle collision) couplings were performed and their results compared.
- Flow type: Steady, isothermal and turbulent (using SST turbulence model) properties were selected for the flow.
- Number of simulation particles: As consulted with Mansouri et al. [1] around 50,000 particles need to be simulated for particle number independent results. However, to ensure this independency, 100,000 particles were used by this study.

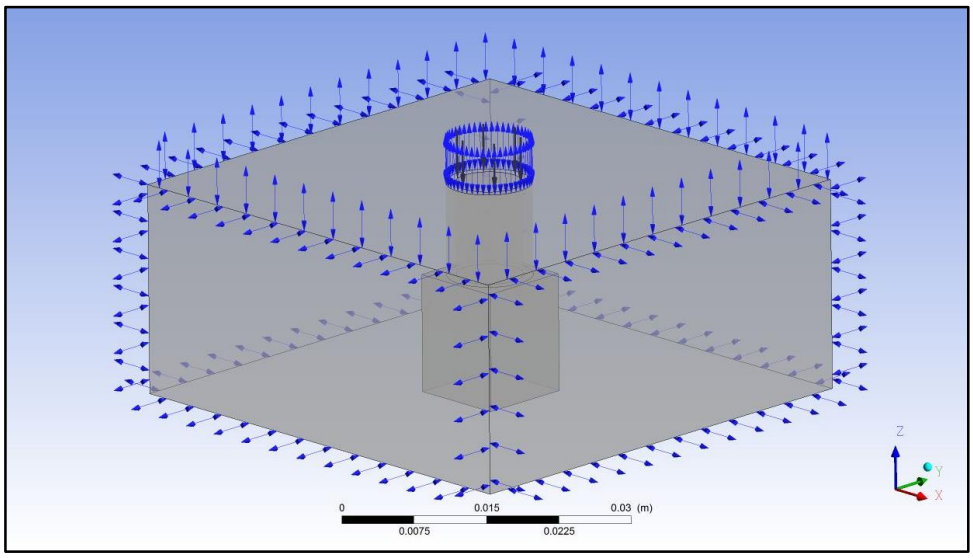

Fig. 9. CFD Model Boundary Conditions - Schematic

3.3.4. Solution post processing. After solving the flow, it is necessary to extract the needed results. ANSYS software provides tools to attain the needed plots and data. However, calculating the erosion profile was not straightforward because ANSYS offers the solution for erosion rate density instead of eroded thickness. Consequently, it was calculated using dimensional analysis as the following equation:

$$Eroded\ Thickness = \frac{Erosion\ Rate\ Density\ \times Test\ Duration}{\rho_p} \qquad (49)$$

where, test duration was taken to be 6h based on experimental work of Mansouri et al. [1]. After calculating the eroded thickness, it was necessary to extract its values over the coupon surface and plot them. This was done by taking circular data samples on the coupon surface, and then averaging the extracted eroded thickness values over the angles for each radius. An algorithmic code was developed using MATLAB software to perform the needed averaging; (See Appendix A for the code).

Similarly, the velocity components of particles at the surface were averaged using another developed MATLAB code (check Appendix A), and then a third code (also provided in Appendix A) was established to calculate from the components the averaged impact velocities and angles of particles across the coupon. These parameters will help better understand the behavior of particles when colliding with the surface, and will thus enhance the comprehension of the erosion profile behavior.

Other results were established directly using ANSYS built-in post processing tools.

Chapter 4. Results and Discussion

In this chapter, the mesh independency test of the developed CFD model is first demonstrated. Then, validation of achieved results is illustrated to make sure the CFD model is working properly. Finally, results and discussion of the intended parametric study are presented.

4.1. Mesh Independency Test

As mentioned earlier, it is very important to check whether the results of the developed CFD model are not dependent on the mesh size. Consequently, three different mesh sizes were considered (refer to Table 4) and their results were compared to select the mesh that offers an independent converged solution. The flow considered for this test was the basic flow (refer to Subsection 3.1.1.) in which one-way coupling was implemented as suggested by [1,21,43] for low concentration slurry flows.

Table 4: Tested Mesh Sizes.

Mesh Name	Mesh Size (Number of Elements)
M0	114,678
M1	277,417
M2	1,654,810

To be able to determine at which mesh size the solution becomes independent, the axial velocity (with respect to the nozzle) and turbulent kinetic energy profiles at three locations away from the coupon were investigated.

Fig. 10 shows a comparison between the axial velocity profiles for the three meshes at the three different locations from the coupon. It can be seen that there is not much of a difference between the results of *M1* and *M2*. Thus, it can be safely concluded that independency is achieved by *M1* for this case.

Additionally, Fig. 11 shows the turbulent kinetic energy profiles by the three meshes at three different locations. Similar to the axial velocity, the results between *M1* and *M2* are very close. As a result, mesh independency is achieved by *M1* for this case too.

In conclusion, three different mesh sizes were compared and their specifications are outlined in Table 4. The comparison was performed by comparing axial velocity and turbulent kinetic energy profiles at three different locations from the coupon surface. It was subsequently found that the *M1* mesh provides independent results in both cases, and thus can be assumed to be the mesh independent size. Consequently, this mesh size was initially selected as the adapted size for this study. However, it was later decided to increase the area of refinement in the jet spread region over the coupon (i.e. the refining box in Fig. 7) to better capture the erosion profile as it is the main concern of this study. As a result, the mesh size increased from 277,417 to 469,886 elements, and was adapted throughout the remainder of the study.

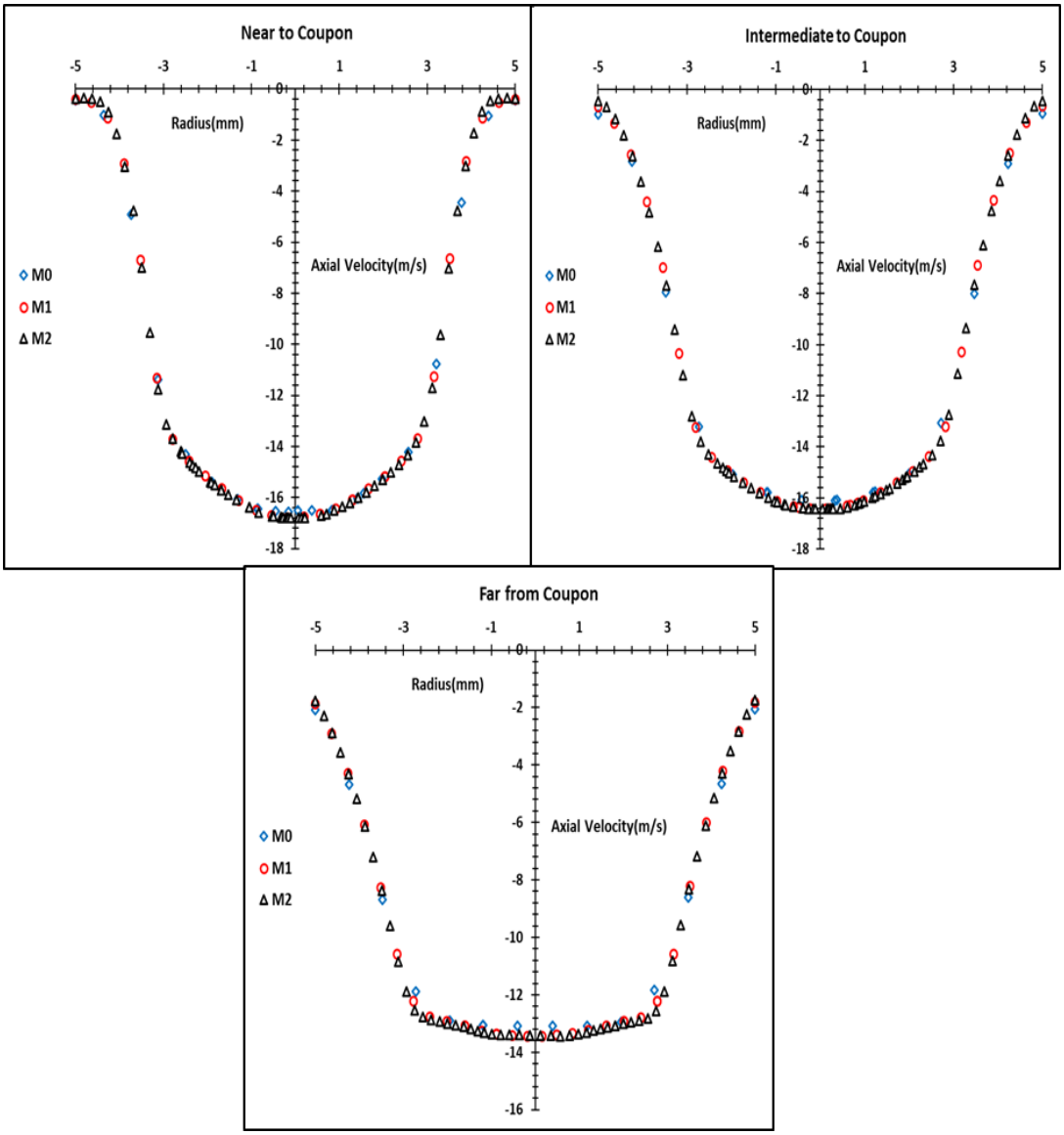

Fig. 10. Axial Velocity Profiles by Three Meshes.

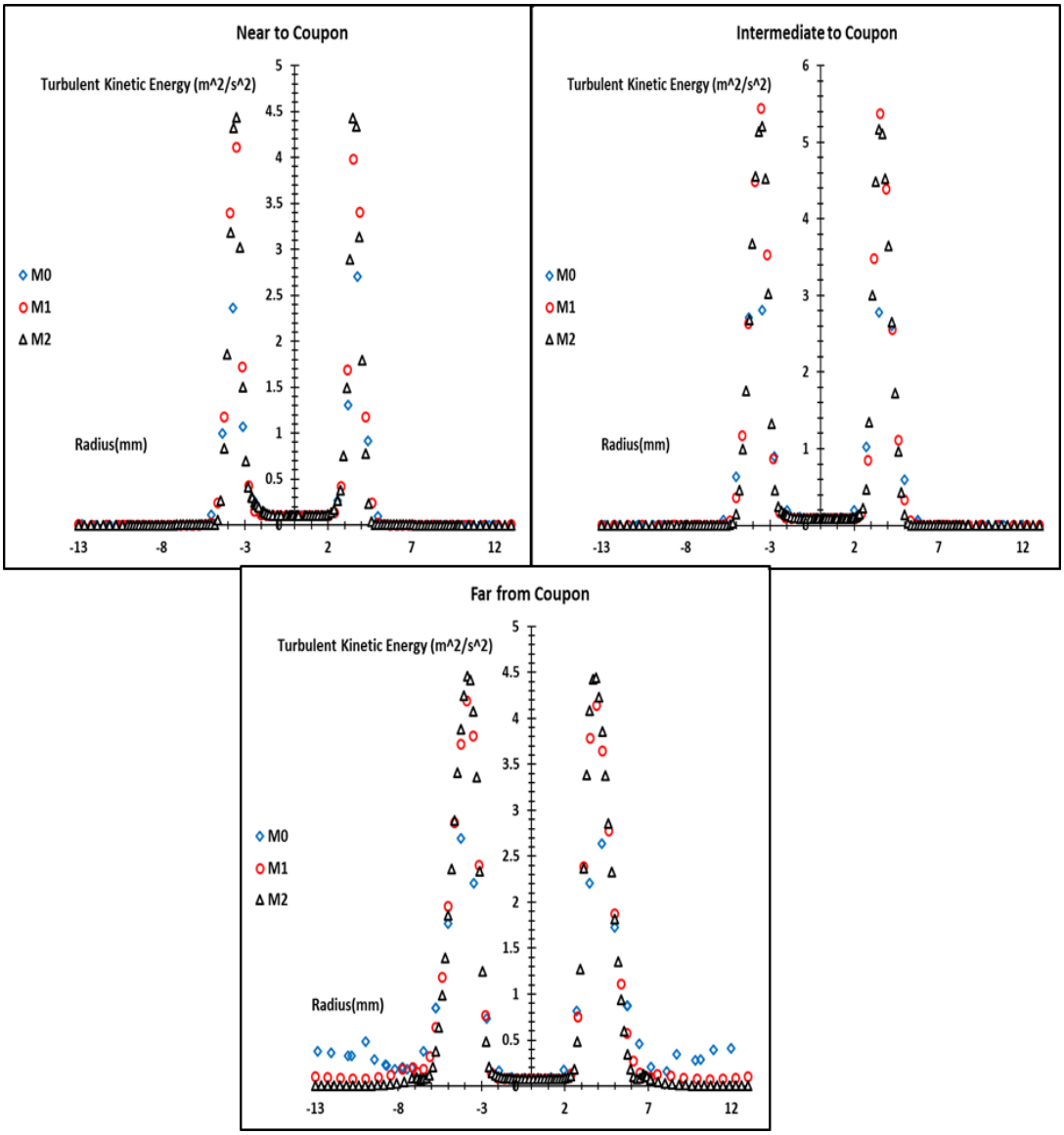

Fig. 11. Turbulent Kinetic Energy Profiles by Three Meshes.

4.2. Validation and Verification of Developed CFD Model

The results from the developed CFD model were compared to those of Mansouri et al. [1] (as it is the basis of this study) to validate the performance of the model. Three different modeling techniques were implemented to the basic flow (see Section 3.1.1.) in order to calculate the resulting erosion profile. These are one-way, two-way and four-way coupling methods. It is suggested by literature that for low particle concentrations, it is enough to perform one-way coupling [1,21,43]. However, it was found by this study that ANSYS CFX requires four-way coupling at all concentration levels to effectively capture the erosion profile; the reason behind this may be attributed to the high density of sand particles as compared to water. This can be seen in Fig. 12, where

one-way and two-way coupling methods result in secondary peaks away from the primary peaks which cannot be validated by literature; check [1,21,22,43].

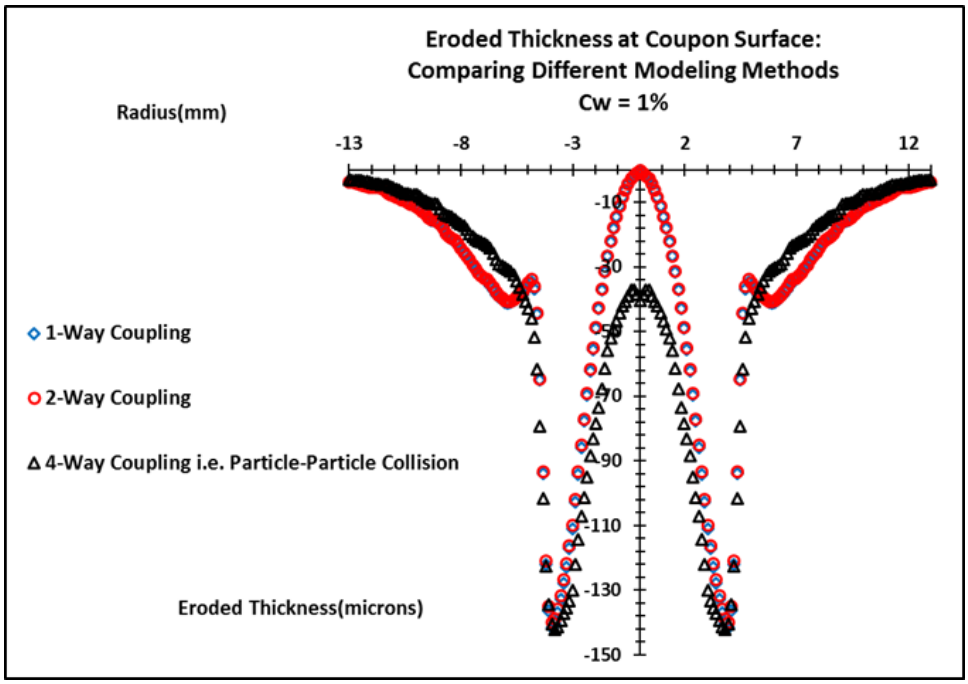

Fig. 12. Comparing Different Modeling Methods for Basic Flow.

Additionally, comparing results of Mansouri et al. [1] in Fig. 13 with results by the current study's four-way coupling method, they were found to be very close, and have the W-shape profile associated with ductile materials eroded in a direct jet impingement setup. However, at the coupon center, the current study exhibits a non-zero erosion magnitude, which differs from [1] in Fig. 13. This is because the current study assumes the nozzle and coupon are not submerged in water, in contrast to Mansouri et al. [1], which consequently results in this higher erosion at the center. This aspect of non-submerged setup was also demonstrated by [21,22,43] where non-zero erosion is found at the coupon center. However, to further confirm this aspect, the experimental non-submerged specifications from Wang et al. [21] were implemented to the current developed CFD setup (with four-way coupling technique), and their results were compared as seen in Fig. 14. The experimental specifications adopted from Wang et al. [21] with some assumptions were as the following:

- Slurry flow of water carrying sand particles
- Direct jet impingement setup as in Fig. 5
- Impingement angle: 90º; i.e., the nozzle is normal to the target (coupon) surface

- Nozzle diameter: 4.8mm
- Stand-off distance (distance between nozzle and coupon): 18.5mm
- Nozzle average velocity (U): 9m/s
- Coupon material: Stainless steel 304
- Sand particle diameter (d_p): 300microns
- Sand particle shape: Spherical (assumed)
- Sand particle density: 2650kg/m^3 (assumed)
- Sand particle concentration by weight: 2%
- Test duration: 2h

It can be clearly seen from Fig. 14 the existence of a non-zero erosion value at the coupon center in non-submerged setups. However, it should be noted that Wang et al. [21] measure the erosion profile along two coupon axes (x and y) whereas the current study demonstrates the average profile over the whole plane. This in turn could result in the observed magnitude difference between the two profiles. Therefore, it can be safely considered that the current developed CFD model is producing valid results.

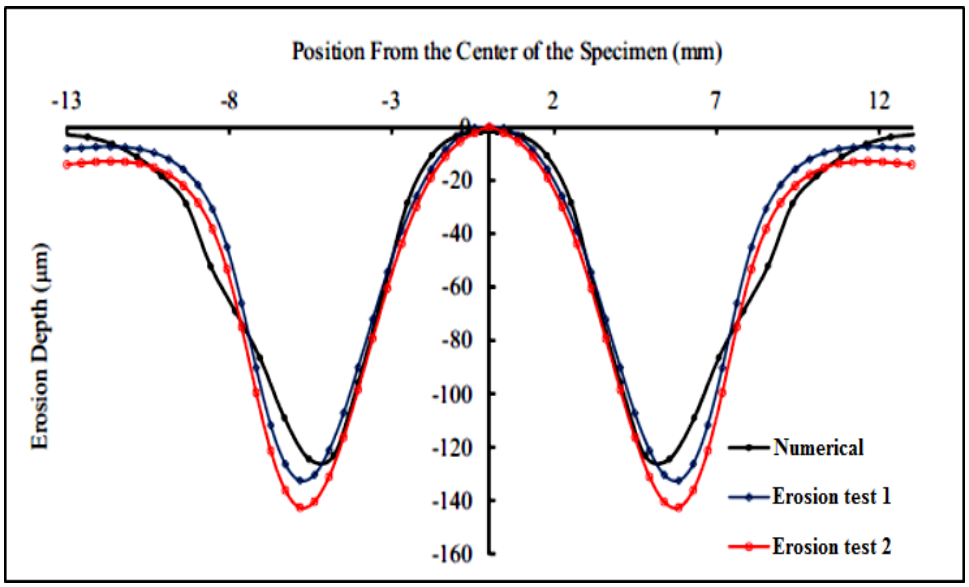

Fig. 13. Erosion Profiles by Mansouri et al. [1].

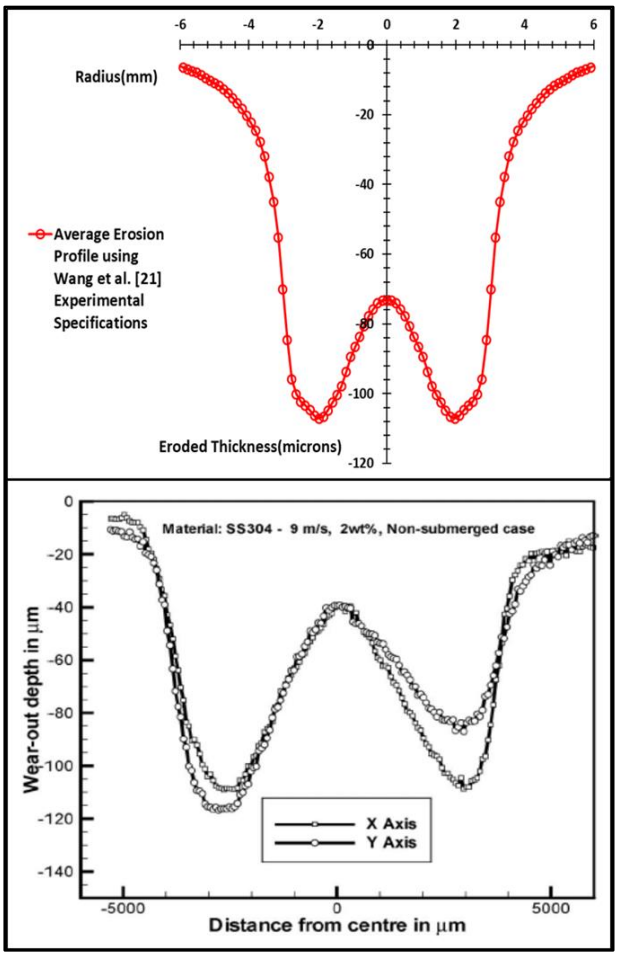

Fig. 14. Comparison of Erosion Profiles in Non-submerged Setup: Current Developed CFD Setup (Top) and Wang et al. [21] Experimental Setup (Bottom).

Therefore, four-way coupling can be considered as the valid modeling method for the fluid flow under analysis as its results are close to that by Mansouri et al. [1] and Wang et al. [21]. Corresponding to this, the CFD model, considered for the parametric analysis of this study, was selected to implement four-way coupling to take into consideration the effect of particle-particle collision on the motion of particles and continuous medium. However, it is important to emphasize that the specifications by Mansouri et al. [1] were selected to be adopted throughout the remainder of this study.

In addition, the results by ANSYS CFX have been tested for verification to ensure that produced erosion profile is corresponding to the model described by Equations 47 and 48. Consequently, the function of impact angle and erosion profile has been calculated (check Appendix A for the algorithm) from the average impact velocities and angles of particles at the coupon surface, and then compared with material impact angle characteristics from Fig. 4 and current erosion profile (four-way coupling); respectively. The plots in Fig. 15 show that the range of impact angles

corresponding to maximum function of impact angle (and thus maximum erosion) is between 10º-30º, which agrees with the impact angle characteristics of ductile material shown in Fig. 4. Moreover, the calculated normalized erosion profile in Fig. 15 shows similar pattern and peak locations to that by the current study (Fig. 12). However, the calculated profile is not smooth because it was based on the average impact velocities and angles of particles, and thus the effect of all hitting particles was not taken into account. This further confirms the verified performance of the achieved CFD model with four-way coupling.

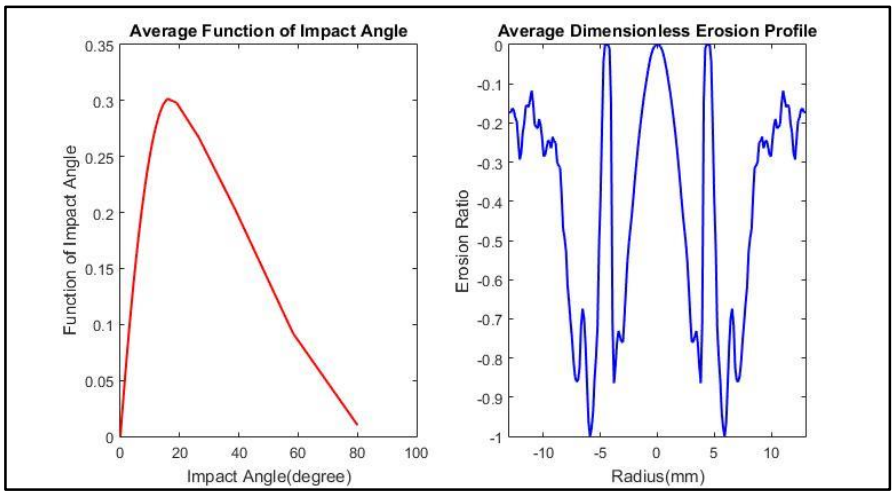

Fig. 15. Calculated Average Function of Impact Angle and Dimensionless Erosion Profile.

4.3. Parametric Study

4.3.1. Overview of study. A list of the performed parametric study points can be described as the following:

- Study the effect of solid particle concentration on erosion profile:
    - Four concentration values were evaluated while fixing all other erosion controlling parameters:
        a. Cw = 1% i.e. Cv = 0.38%
        b. Cw = 8% i.e. Cv = 3.18%
        c. Cw = 15% i.e. Cv = 6.24%
        d. Cw = 22% i.e. Cv = 9.62%
- Study the effect of Stokes number on erosion profile by varying three of its defining parameters (check Equations 1 and 2):

- Each time one parameter is varied while fixing all other parameters for three Stokes numbers (2.98, 29.8 and 298) as the following:
    a. Changing solid particle diameter ➔ d_p = [94.9, 300, 949]microns
    b. Changing nozzle average velocity ➔ U = [1.4, 14, 140]m/s
    c. Changing fluid dynamic viscosity ➔ μ = [8.893, 0.8899, 0.08893]cp

- Check if there is an effect of concentration on the way Stokes number affects the erosion profile:
    - The is done by evaluating the values of the Stokes number defining parameters for low and high solid particle concentration levels ➔ Cw = 1% and 22% i.e. Cv = 0.38% and 9.62%

- A summary of all performed simulation cases is shown in Table 5 (for each case the changing parameter is italicized and bolded):

Table 5: List of All Parametric Study Cases.

Case	***Cw*(%)**	***St***	***d_p*(microns)**	***U*(m/s)**	***μ*(cp)**
1	***1***	29.8	300	14	0.8899
2	***8***	29.8	300	14	0.8899
3	***15***	29.8	300	14	0.8899
4	***22***	29.8	300	14	0.8899
5	***1***	***2.98***	***94.9***	14	0.8899
6	***1***	***298***	***949***	14	0.8899
7	***22***	***2.98***	***94.9***	14	0.8899
8	***22***	***298***	***949***	14	0.8899
9	***1***	***2.98***	300	***1.4***	0.8899
10	***1***	***298***	300	***140***	0.8899
11	***22***	***2.98***	300	***1.4***	0.8899
12	***22***	***298***	300	***140***	0.8899
13	***1***	***2.98***	300	14	***8.893***
14	***1***	***298***	300	14	***0.08893***
15	***22***	***2.98***	300	14	***8.893***
16	***22***	***298***	300	14	***0.08893***

4.3.2. Results and analysis. The results from the parametric study and highlights of important analytical points are presented in this subsection.

4.3.2.1. *Changing solid particle concentration.* The first thing that can be depicted from Fig. 16A is that as the solid particle concentration increases, the erosion magnitude also increases. This is because with higher concentration, more particles hit the surface of the coupon resulting in greater thickness loss. However, looking at Fig. 16B, one can better understand what happens to the erosion pattern when concentration is increased. It can be seen that as the concentration increases, the drop in erosion after the peak (away from coupon's center) is much steeper indicating that the solid particles are becoming less entrained by the fluid flow. This resistance occurs because as the concentration increases, the solid particles become more heavily packed thus decreasing the capability of the fluid to penetrate the distances between the particles and affecting their motion. Consequently, the spreading of the particles away from the coupon's center decreases with higher concentration.

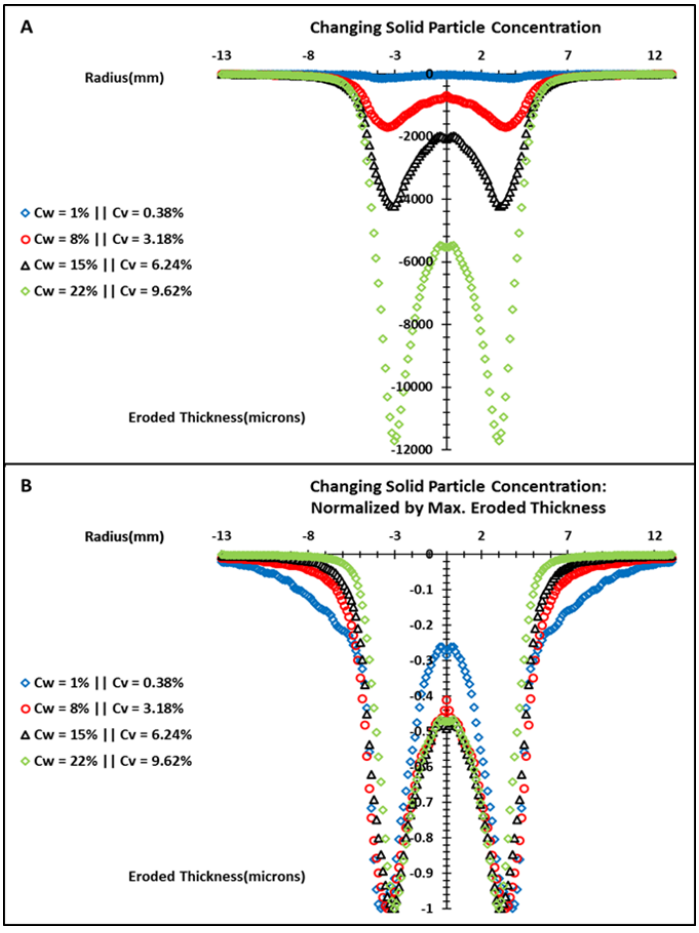

Fig. 16. Comparison of Erosion Profiles when Changing Solid Particle Concentration: (A) Actual Profiles and (B) Normalized Profiles by Maximum Eroded Thickness in Each Case.

Additionally, the ratio of central erosion depth to peak erosion depth increases with higher concentration, as seen in Fig. 16B. However, this increase tends to reach a saturation level at high concentration values (Cv = 6.24% and Cv = 9.62%). This can be attributed to the fact that with higher concentration, particles at the surface create a shielding zone (as was explained in Chapter 2), which decreases the velocity of subsequent impacting particles, and thus decreasing their erosion effect. This can be clearly seen in Fig. 17A where the average impact velocity of particles drops with the increase in concentration. Therefore, it cannot be concluded that with higher concentration, the erosion profile in slurry flows changes from a W-shape to U-shape like in dry flows.

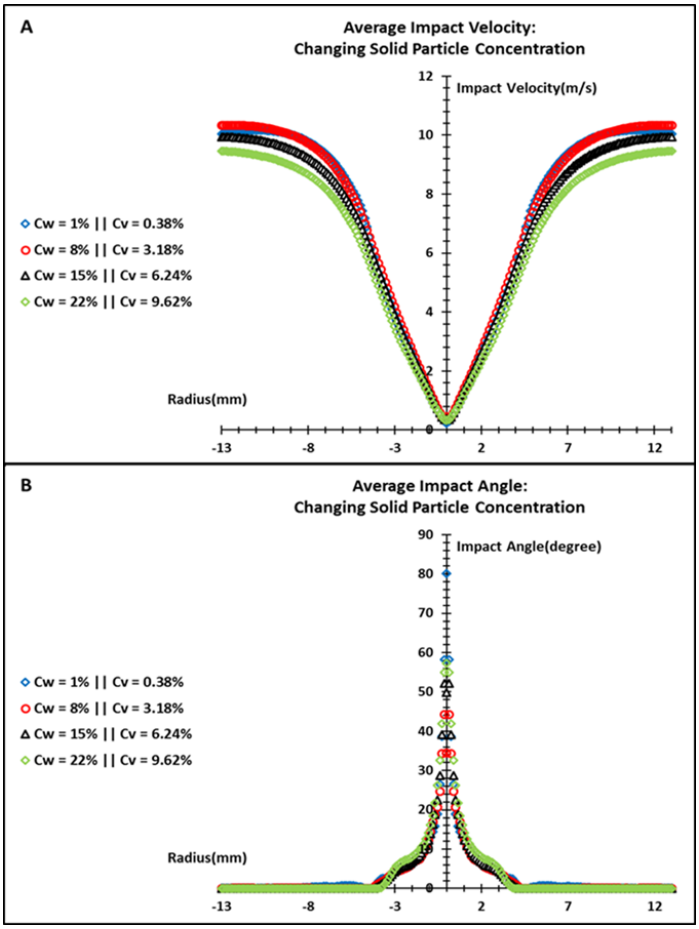

Fig. 17. Comparison of (A) Average Impact Velocity and (B) Average Impact Angle when Changing Solid Particle Concentration.

Furthermore, Fig. 17B shows that as the concentration increases, more particles hit the central region with erosive average impact angles. This corresponds to the previous explanation that with increase in concentration, particles become less

entrained by the fluid; hence, they impact the central region with higher frequency than away.

To conclude, as solid particle concentration increases, erosion magnitude increases whereas erosion spread decreases due to the resistance of particles to fluid motion.

4.3.2.2. *Changing solid particle diameter.* This was done at two concentration levels: low (Cw=1% i.e. Cv=0.38%) and high (Cw=22% i.e. Cv=9.62%).

4.3.2.2.1. *At low concentration.* Looking at Fig. 18A it can be noticed that as the solid particle diameter decreases, the erosion magnitude increases. This contradicts with literature, which indicates that the bigger the particle size is, the more erosion it will cause [42]. However, this unexpected result highlights an important aspect in slurry flows: although particle size is an important determinant of erosion magnitude, the interaction between particles and fluid is even more important. In relation to that, it can be deduced that particles with smaller size have lower inertia meaning that they can be entrained and speeded up by the fluid more easily. Consequently, they will have higher impact speeds, which in turn increase the erosion magnitude. This can be clearly seen in Fig. 19A where particles with smaller diameter have considerably higher average impact velocities at all locations .

Additionally, this higher entrainment of smaller particles by the fluid can be better seen in Fig. 18B where the erosion profile corresponding to the smallest particle diameter has a bigger erosion spread away from the coupon's center; this spread decreases with higher particle sizes.

The decrease in entrainment, as the particle size increases, causes more erosion depth in the central region as well as greater ratio of central erosion depth to peak erosion depth. This is because with less entrainment, a higher number of particles hit the central region with erosive impact angles causing more erosion. Therefore, the erosion profile starts to shift from a W-shape to a U-shape, as expected, with increase in Stokes number by increasing particle size. Fig. 19B supports this analysis by demonstrating that larger particles tend to hit the central region with erosive average impact angles more than they do further away.

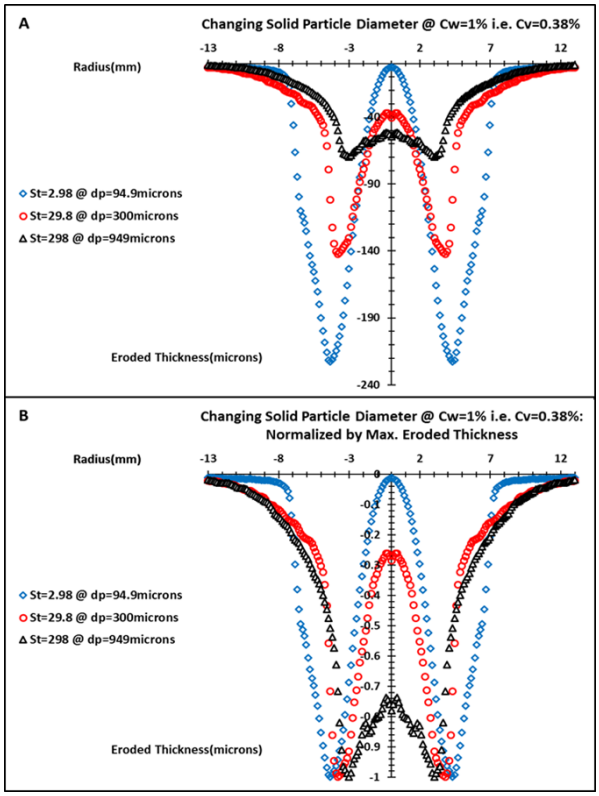

Fig. 18. Comparison of Erosion Profiles when Changing Solid Particle Diameter at Low Solid Particle Concentration: (A) Actual profiles and (B) Normalized Profiles by Maximum Eroded Thickness in Each Case.

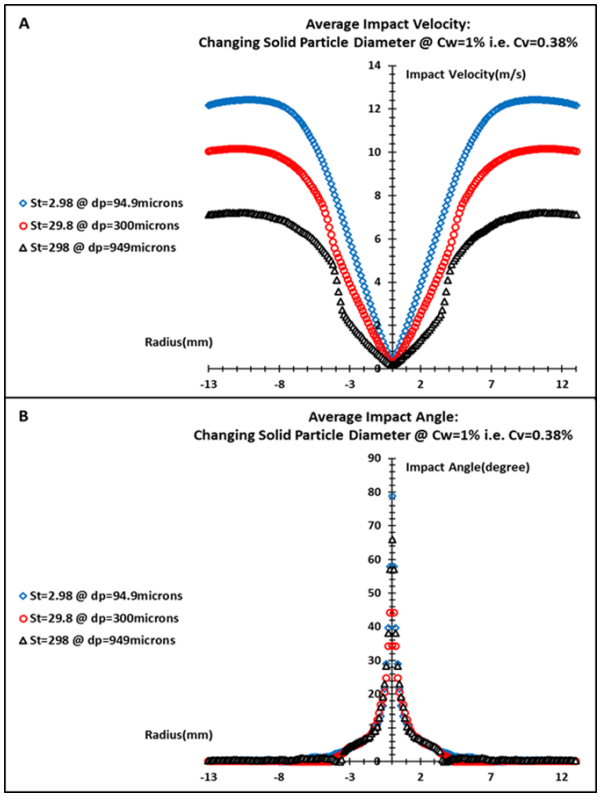

Fig. 19. Comparison of (A) Average Impact Velocity and (B) Average Impact Angle when Changing Solid Particle Diameter at Low Solid Particle Concentration.

In summary, at low solid particle concentration, the erosion magnitude decreases with increase in particle size due to the lower entrainment of particles by the fluid. However, as the Stokes number increases by increasing the particle size, the erosion profile in slurry flow starts inheriting that corresponding to a dry flow.

4.3.2.2.2. *At high particle concentration.* At high solid particle concentration, the effect of particle diameter is not as clear as that at low concentration. The erosion magnitude tends to increase with increase in particle size up to a certain threshold and then starts decreasing back with larger particle diameters; see Fig. 20A. This can be understood by considering two aspects: impact velocity and impact angle.

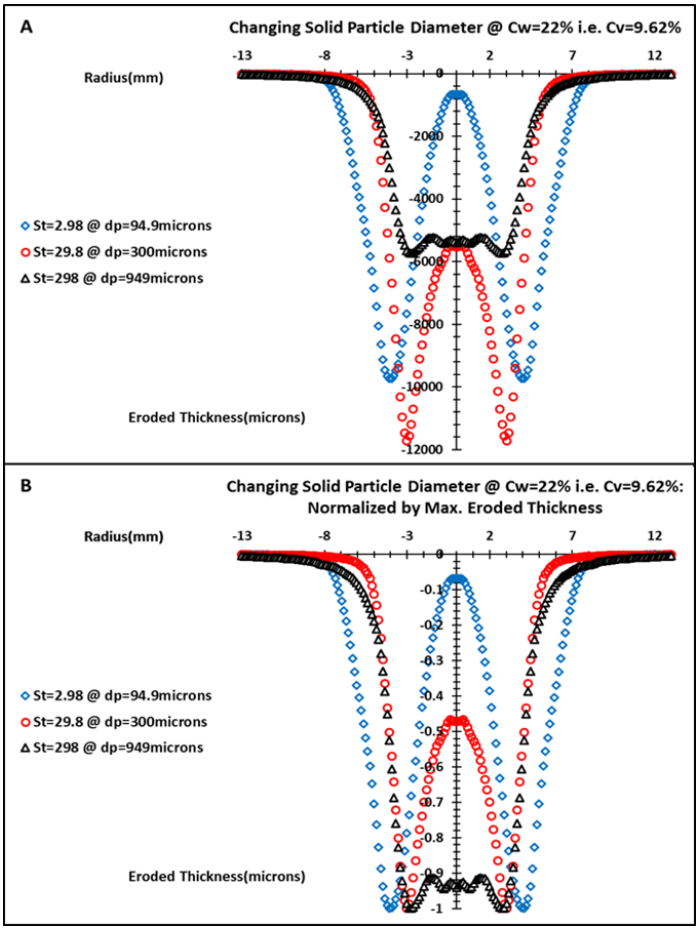

Fig. 20. Comparison of Erosion Profiles when Changing Solid Particle Diameter at High Solid Particle Concentration: (A) Actual Profiles and (B) Normalized Profiles by Maximum Eroded Thickness in Each Case.

At high solid particle concentration, particles are more closely packed together thus interacting more with one another and, as previously mentioned, smaller particles can be more entrained and speeded up by the fluid than larger particles. This will cause smaller particles to interact with each other in a more aggressive way than that at low

concentration. Therefore, they lose some of their kinetic energy and momentum due to their higher interaction frequency. This can be clearly seen for particles with 94.9 and 300 microns diameters when comparing Figs. 19A and 21A, where the average impact velocity of particles decreases as the concentration increases for same particle sizes. Additionally, looking at Fig. 21B, it can be noticed that particles with 300 microns diameter having average impact angles of around 10º-20º are more than 94.9 microns particles in the peak erosion depth region. This is because smaller particles have higher interaction frequency which distributes their impact angle values on a more diverse range. As a result, despite that 94.9 microns particles have higher average impact velocity, 300 microns particles cause greater erosion as more particles have average impact angles of around 10º-20º; which is a range corresponding to greater erosion, (See Fig. 15).

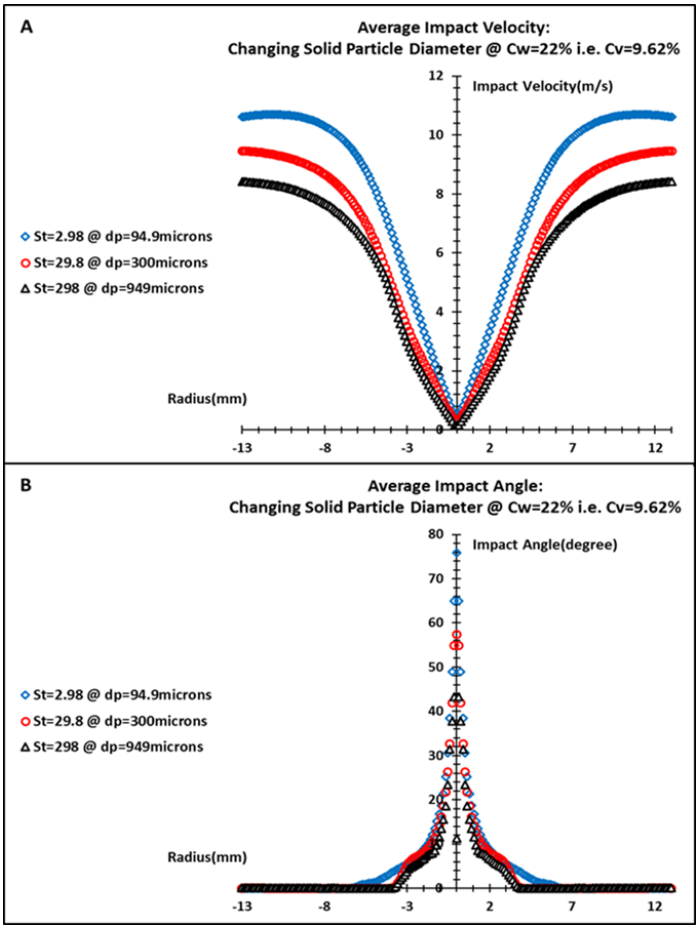

Fig. 21. Comparison of (A) Average Impact Velocity and (B) Average Impact Angle when Changing Solid Particle Diameter at High Solid Particle Concentration.

However, as the particle size further increases (from 300 to 949 microns), the erosion magnitude decreases. This is because, as their size increases, particles interact

with each other in a less aggressive way at high concentration than smaller particles; their interspatial distances are smaller. Thus, their impact behavior remains relatively the same as in low concentration case; hence, the decrease in erosion magnitude occurs with an increase in particle size; which is mainly governed by the decrease in impact velocity.

Furthermore, at high concentration, the effect of particle size on erosion profile shape is the same at low concentration. As the Stokes number increases by increasing the particle diameter, the fluid less entrains the particles and thus the erosion spread decreases; (See Fig. 20B). Additionally, the ratio of central erosion depth to peak erosion depth increases with particle size because more particles hit the central region with erosive impact angles, (See Fig. 21B), causing the erosion profile to change from W-shape to U-shape like that in dry flow.

In conclusion, at high concentration, the erosion magnitude increases and then decreases with an increase in particle diameter. This initial increase is mainly due to the more aggressive interaction between smaller particles. However, similar to the low concentration case, the erosion profile approaches that of a dry flow by increasing the Stokes number when increasing the particle size.

4.3.2.3. ***Changing nozzle average velocity.*** This was done at two concentration levels: low (Cw=1% i.e. Cv=0.38%) and high (Cw=22% i.e. Cv=9.62%).

4.3.2.3.1. *At low concentration.* Fig. 22A, B and C demonstrate that at low solid particle concentration, as the nozzle average velocity increases, the erosion magnitude increases. This agrees with literature, as shown in Chapter 2, because an increase in nozzle velocity correlates to an increase in particle impact velocity (see Fig. 23A); thus, the increase in erosion.

Moreover, looking at Fig. 22D, the change in erosion profile shape with nozzle velocity can be better understood. The higher the nozzle velocity, the narrower the fluid jet diameter is. Consequently, the erosion spread becomes narrower and the ratio of central erosion depth to peak erosion depth becomes larger as more particles hit the coupon's central region. This decrease in spread can also be seen in Fig. 23B where the average impact angle drops to zero away from the peak region. However, an interesting behavior should be highlighted that the erosion profile shape stops changing with higher nozzle velocities, which can be seen as the minimal difference between the profile at

U=14m/s and *U*=140m/s; Fig. 22D. Thus, it cannot be concluded that the profile is becoming like that of a dry flow when increasing the Stokes number by increasing the nozzle velocity at low concentration.

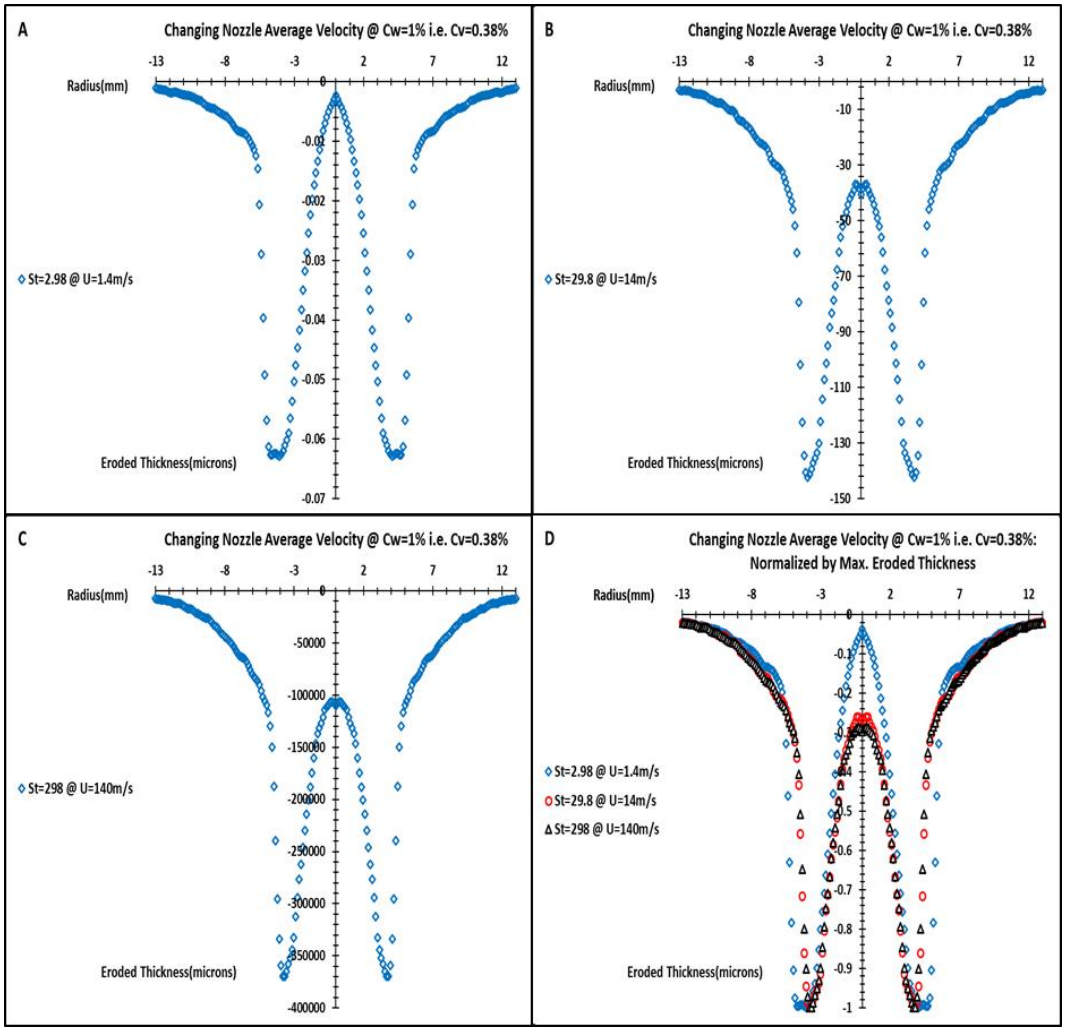

Fig. 22. Comparison of Erosion Profiles when Changing Nozzle Average Velocity at Low Solid Particle Concentration: (A), (B), (C) Actual Profiles and (D) Normalized Profiles by Maximum Eroded Thickness in Each Case.

Moreover, looking at Fig. 22D, the change in erosion profile shape with nozzle velocity can be better understood. The higher the nozzle velocity, the narrower the fluid jet diameter is. Consequently, the erosion spread becomes narrower and the ratio of central erosion depth to peak erosion depth becomes larger as more particles hit the coupon's central region. This decrease in spread can also be seen in Fig. 23B where the average impact angle drops to zero away from the peak region. However, an interesting behavior should be highlighted that the erosion profile shape stops changing with higher nozzle velocities, which can be seen as the minimal difference between the profile at *U*=14m/s and *U*=140m/s; Fig. 22D. Thus, it cannot be concluded that the profile is

becoming like that of a dry flow when increasing the Stokes number by increasing the nozzle velocity at low concentration.

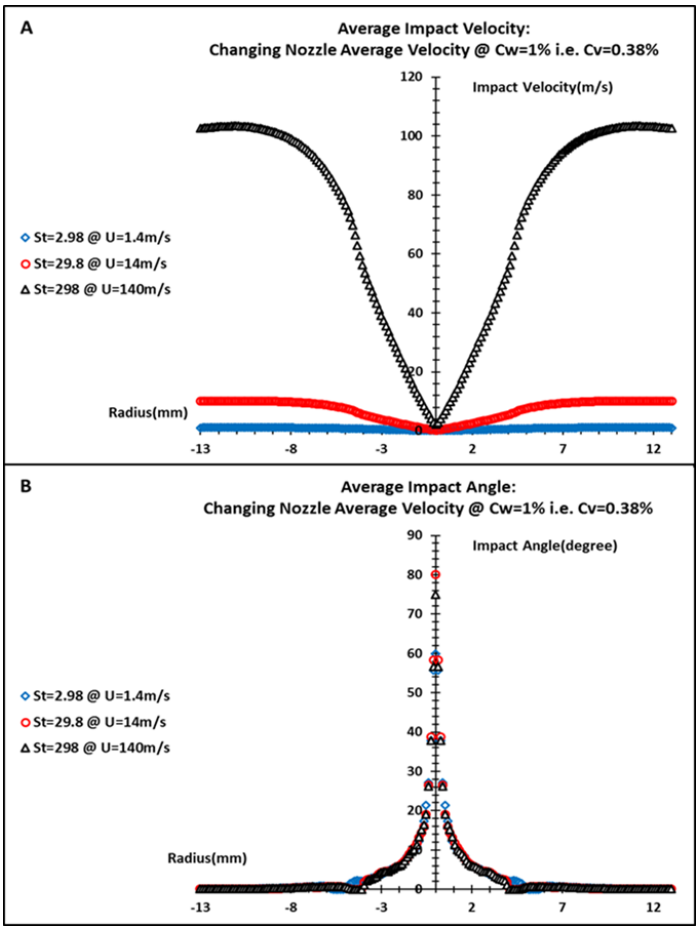

Fig. 23. Comparison of (A) Average Impact Velocity and (B) Average Impact Angle when Changing Nozzle Average Velocity at Low Solid Particle Concentration.

In summary, at low particle concentration, an increase in Stokes number by increasing average nozzle velocity causes higher erosion magnitude due to the associated higher impact velocity. Additionally, the fluid has a smaller jet diameter causing narrower erosion spread away from coupon center. However, the erosion profile growth tends to saturate at high Stokes numbers preventing the profile from changing to a U-shape like that in a dry flow.

4.3.2.3.2. *At high concentration.* As can be seen from Fig. 24A, B and C, similar to low concentration, increasing the nozzle average velocity at high concentration increases the erosion magnitude. This is, as mentioned earlier, due to the subsequent increase in particle impact velocity; see Fig. 25A.

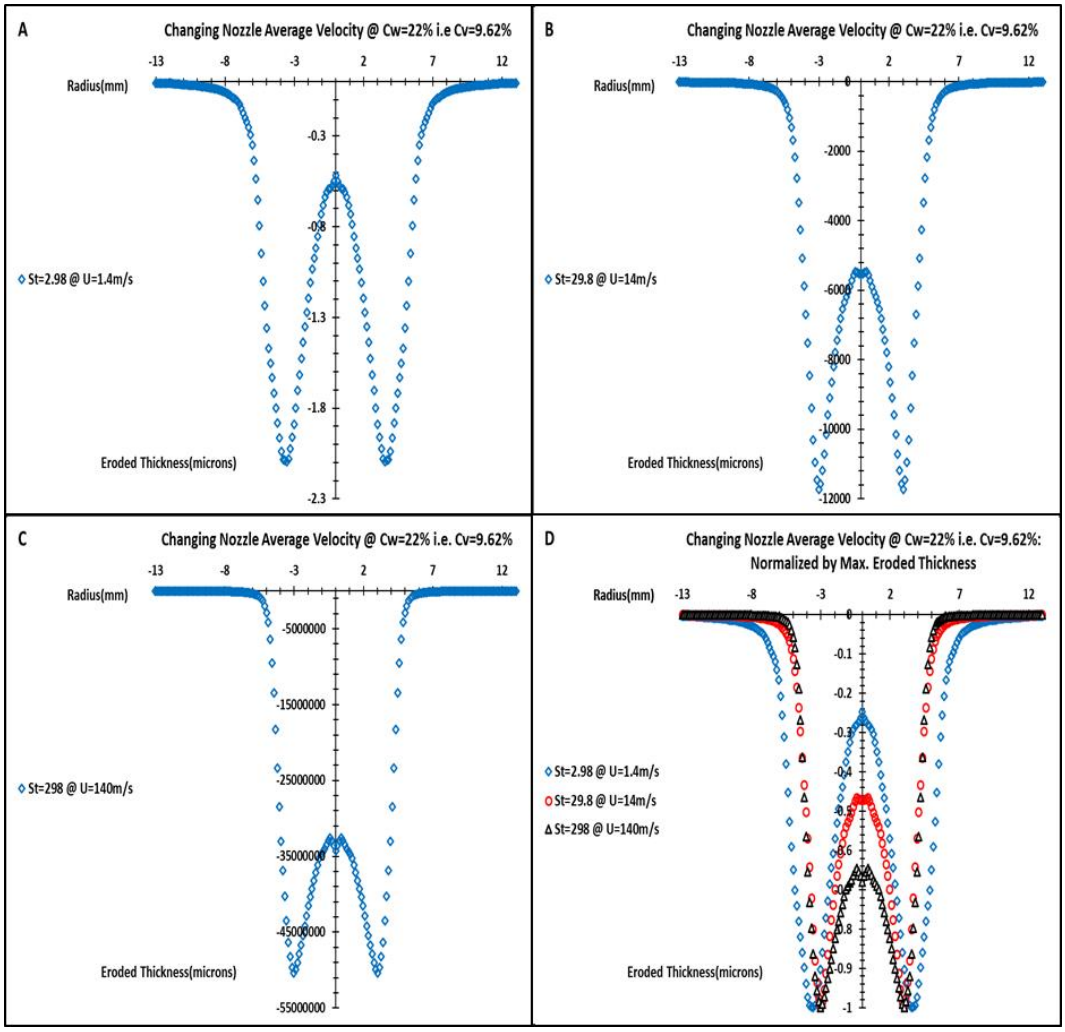

Fig. 24. Comparison of Erosion Profiles when Changing Nozzle Average Velocity at High Solid Particle Concentration: (A), (B), (C) Actual Profiles and (D) Normalized Profiles by Maximum Eroded Thickness in Each Case.

However, the significant difference in this case is that the erosion profile continues to grow from a W-shape to a U-shape as seen in Fig. 24D. This indicates that at high concentration, the Stokes number has more influence on the erosion profile than that at low concentration when changing the nozzle average velocity. This can be explained by the fact that; at high concentration, particles are heavily packed to each other, and as mentioned earlier, this resists the fluid entrainment on the particles. Consequently, particles will hit the center at a much higher frequency and with a bulkier stack than in low concentration case. Therefore, the change in ratio of central erosion depth to peak erosion depth is more profound at high than low concentration in which particles tend to hit the surface with less bulkiness. This can be better deduced by comparing Fig. 23B with Fig. 25B in which particles at high concentration tend to resist

more the fluid motion, and thus have more erosive average impact angles around the central region than at low concentration.

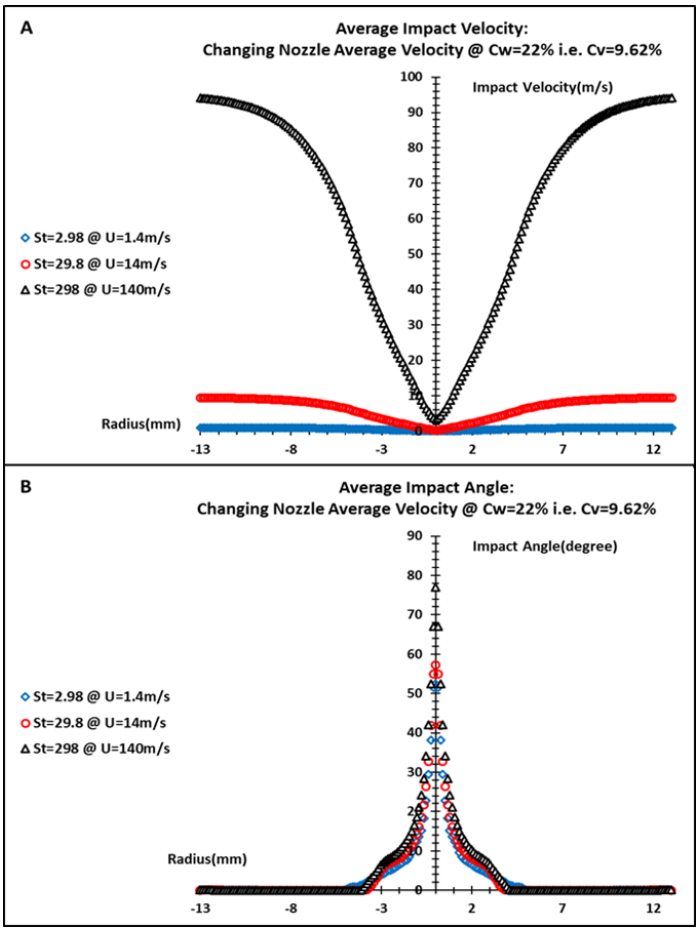

Fig. 25. Comparison of (A) Average Impact Velocity and (B) Average Impact Angle when Changing Nozzle Average Velocity at High Solid Particle Concentration.

To summarize, at high concentration, the erosion magnitude increases with the increase in Stokes number by increasing the average nozzle velocity. This is similar to the low concentration case. However, at high concentration the effect of Stokes number is more significant than at low concentration, causing the profile to approach a dry flow shape.

4.3.2.4. *Changing fluid dynamic viscosity.* This was done at two concentration levels: low (Cw=1% i.e. Cv=0.38%) and high (Cw=22% i.e. Cv=9.62%).

4.3.2.4.1. *At low concentration.* Fig. 26A suggests that, at low particle concentration, as the Stokes number increases by decreasing the fluid viscosity, the erosion magnitude tends to decrease. As explained by Mansouri et al. [42], as the fluid viscosity increases, the flow in the nozzle becomes more laminar which in turn causes

the velocity profile at the exit to be parabolic. Consequently, a parabolic profile has higher particle velocities at the nozzle center than a turbulent profile, which in turn results in higher particle impact speeds. This can be further seen in Fig. 27A where the average impact velocity of solid particles increases with higher viscosity, and thus the erosion magnitude increases too. However, the magnitude tends to saturate at low fluid viscosities as seen at μ=0.8899cp and μ=0.08893cp. This is because the corresponding average impact velocities and angles are almost identical at low viscosities; see Fig. 27A and B.

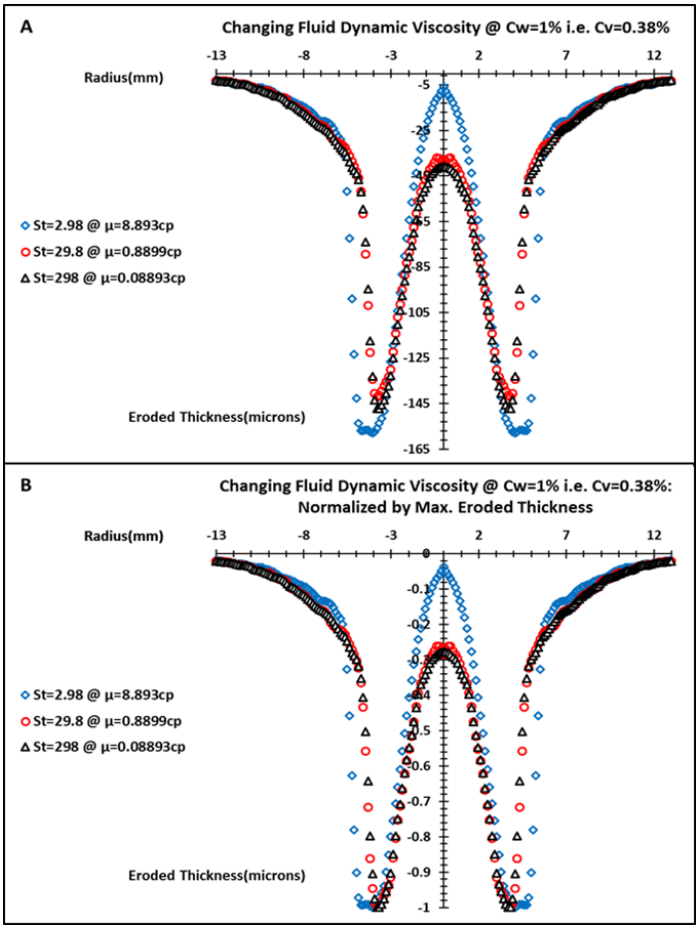

Fig. 26. Comparison of Erosion Profiles when Changing Fluid Dynamic Viscosity at Low Solid Particle Concentration: (A), (B), (C) Actual Profiles and (D) Normalized Profiles by Maximum Eroded Thickness in Each Case.

Furthermore, the fluid with higher viscosity has a stronger entrainment of particles than lower viscosity fluids, because its viscous effects on particles are greater. This can be clearly seen in Figs. 26B and 27B where the erosion spread away from the coupon center tends to become narrower as the fluid viscosity decreases, and more particles hit the central region with erosive average impact angles. However, this spread tends to reach a saturation point at low fluid viscosities in which the profile stops

changing. Similarly, the ratio of central erosion depth to peak erosion depth increases but reaches a saturation point. Therefore, it cannot be suggested that the erosion profile grows to a U-shape profile as the Stokes number increases by decreasing fluid viscosity for this case.

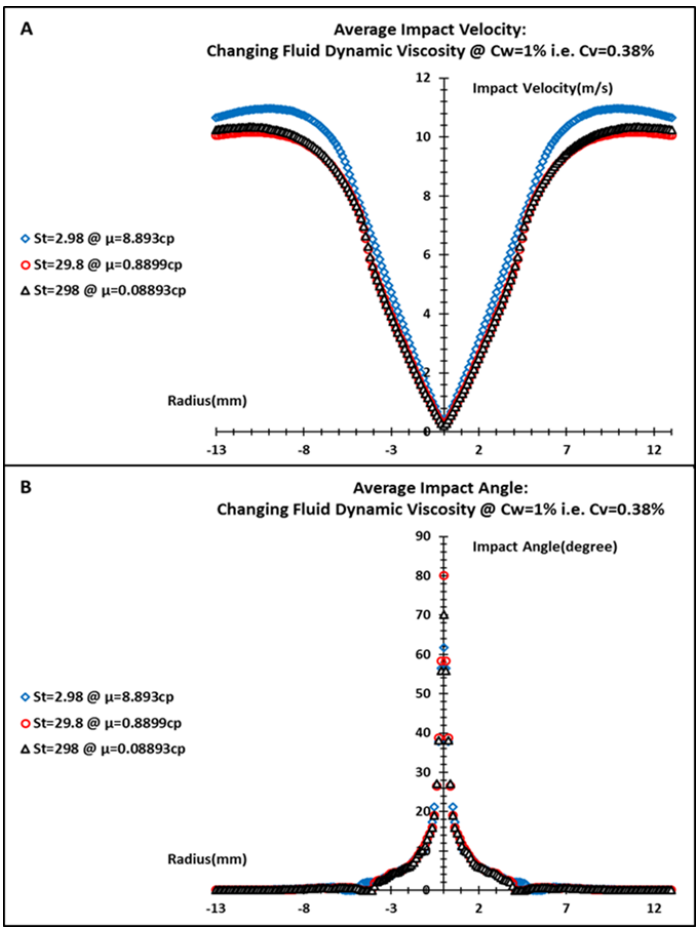

Fig. 27. Comparison of (A) Average Impact Velocity and (B) Average Impact Angle when Changing Fluid Dynamic Viscosity at Low Solid Particle Concentration.

To conclude, at low particle concentration, as the Stokes number increases by decreasing fluid viscosity, the erosion magnitude decreases and reaches a saturation point at low viscosities. Additionally, at high viscosity, the fluid better entrains the particles causing a wider erosion spread. However, the erosion profile cannot be assumed to grow to that of a dry flow as the Stokes number increases.

4.3.2.4.2. *At high concentration.* As noticed in all other cases, at high concentration the behavior of the erosion profile changes. Fig. 28A demonstrates that as the Stokes number increases by decreasing the fluid viscosity, the erosion magnitude increases, which contradicts the results of low concentration case. The reason behind this is that at high concentration, particles are heavily packed together, and thus particle-

particle interaction is greater than at low concentration. Consequently, despite the lower average impact velocity of particles as viscosity decreases (because of the laminar parabolic velocity profile effect previously explained), their average impact angle tends to have greater erosive range in the peak region; see Fig. 29A and B. This in turn, increases the erosion magnitude.

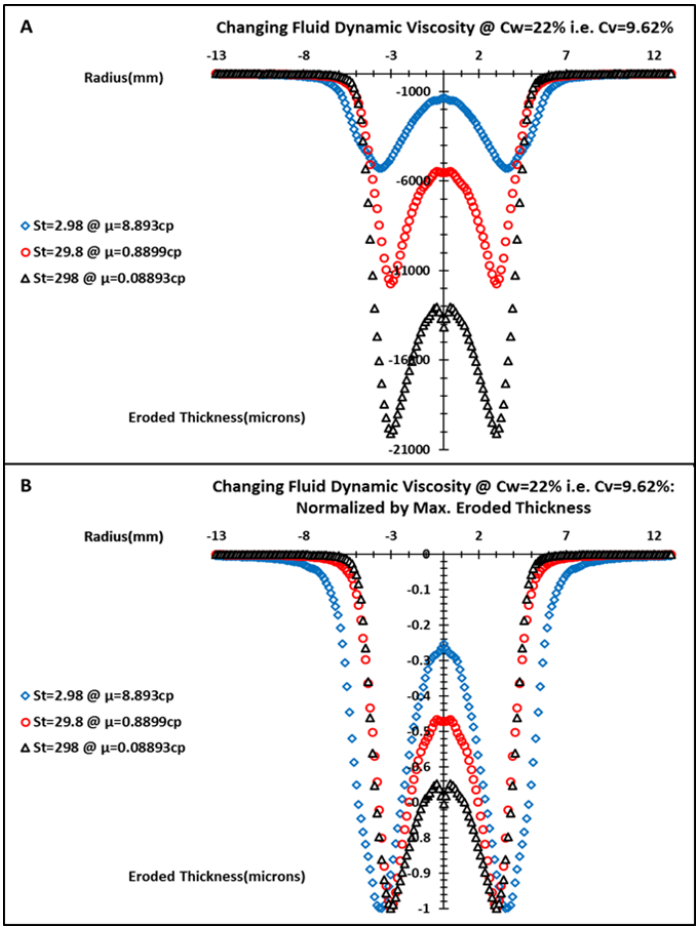

Fig. 28. Comparison of Erosion Profiles when Changing Fluid Dynamic Viscosity at High Solid Particle Concentration: (A), (B), (C) Actual Profiles and (D) Normalized Profiles by Maximum Eroded Thickness in Each Case.

Furthermore, Fig. 28B shows that, unlike low concentration case, at high concentration, the erosion profile tends to grow from a W-shape to U-shape as the Stokes number increases by decreasing fluid viscosity due to the decreased entrainment of particles by the fluid. This indicates that the Stokes number has a higher effect on erosion profile growth when changing fluid viscosity at high concentration. This is because particles approach the central region with a bulkier body causing greater impact frequency than they do at low concentration. Consequently, the ratio of central erosion depth to peak erosion depth changes in a more explicit way than at low concentration case. This can also be seen in Fig. 29B in which particles have more erosive average

impact angles around the central region at lower viscosities than in the low concentration case (see Fig. 27B). Additionally, the erosion spread away from the center gets narrower as the Stokes number increases which is directly related to the decreased entrainment of the particles.

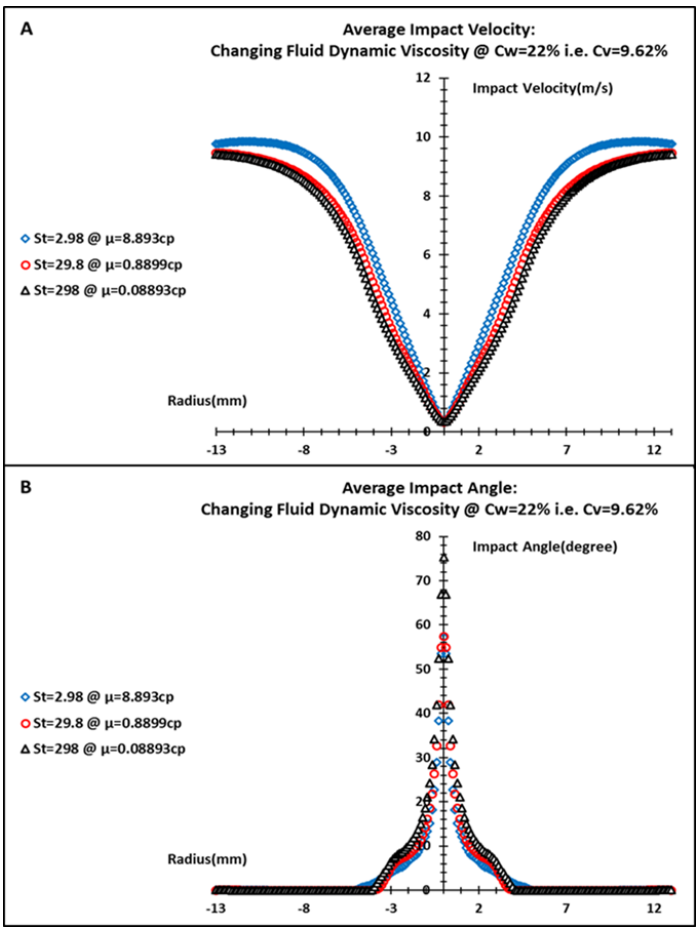

Fig. 29. Comparison of (A) Average Impact Velocity and (B) Average Impact Angle when Changing Fluid Dynamic Viscosity at High Solid Particle Concentration.

In summary, as the Stokes number increases by decreasing fluid viscosity at high particle concentration, erosion magnitude tends to increase. Moreover, the Stokes number has a more influential effect on the erosion profile than in low concentration case. At high concentration, the erosion profile tends to approach that of a dry flow as the Stokes number increases by decreasing the fluid viscosity.

4.3.3. Summary. Changing solid particle concentration affects the erosion profile; however, its effect is greater on the magnitude than the shape of the profile. As concentration increases, the erosion magnitude increases, and the particles become less entrained by the fluid resulting in a narrower erosion spread. However, the change in

erosion profile shape saturates at high concentration levels, and thus it cannot be assumed to develop into a U-shape profile of a dry flow as the concentration increases.

On the other hand, changing the Stokes number has a strong effect on both the erosion profile magnitude and shape. However, this effect depends on which defining parameter is under analysis and at which solid particle concentration value. As mentioned earlier, it is suggested by literature that at high Stokes numbers, the fluid entrainment on particles is small causing the erosion profile in ductile materials to have a U-shape. On the other hand, at low Stokes numbers, fluid entrainment is higher on particles, and thus ductile materials will exhibit a W-shape erosion profile. However, this association between the shape of erosion profile and Stokes number has been found by this study to be true at high solid particle concentration. In contrast, at low concentration the erosion profile shape tends to approach a U-shape but at some point saturates and stops changing regardless of the increase in Stokes number. Therefore, it cannot be considered that at low concentration the erosion profile approaches that of a high Stokes number flow. This was the case in studying nozzle average velocity and fluid viscosity defining parameters. However, analyzing solid particle diameter clearly demonstrates that at both, low and high, particle concentrations, the erosion profile grows from a W-shape to a U-shape as the Stokes number increases. This further implies that the effect of Stokes number on the erosion profile is dependent on two important factors: solid particle concentration and which defining parameter is being varied.

Chapter 5. Conclusion and Future Work

This thesis performed a numerical parametric study of the effect of solid particle concentration and Stokes number on the erosion profile in slurry flow over ductile material for a direct jet impingement setup. A CFD model using ANSY CFX software was developed to perform the numerical study. Solid particle concentration was varied at four different levels; whereas three Stokes numbers were considered and evaluated by changing three of its defining parameters: solid particle diameter, nozzle average velocity and fluid viscosity. Additionally, the Stokes number was evaluated at two extreme particle concentration levels in order to determine any combined effect resulting on the erosion profile.

It was found that concentration heavily affects the magnitude of erosion profile rather than its shape. As concentration increases, the magnitude also increases whereas the shape starts to become that of a high Stokes flow but then saturates. In contrast, the Stokes number effectively influences both the magnitude and shape of the erosion profile. However, this effect was found to be highly dependent on the concentration level and the defining parameter selected for investigation. At low concentration, it was found that the shape of the erosion profile approaches that of a high Stokes flow but stops changing with increase in Stokes number. This behavior was found to be valid only when the nozzle average velocity and fluid viscosity parameters are varied; whereas, for solid particle diameter the shape tends to fully grow into that of a high Stokes flow. However, at high concentration, the profile's shape effectively grows into that of a high Stokes flow as Stokes number is increased by varying any of the three defining parameters. This in turn better agrees with literature regarding the relation between the erosion profile's shape and Stokes number.

As a future work, this parametric study could be extended to different standoff distances between the nozzle and coupon. This in turn affects the solid particles' motion over the coupon, resulting in different erosion behavior. Additionally, different erosion models could be tested in order to find a more accurate prediction of the erosion profile. Another thing that could be done is testing the other Stokes number defining parameters to determine what effect they could result on the erosion profile.

References

[1] A. Mansouri, H. Arabnejad, S. Shirazi and B. McLaury, "A Combined CFD/Experimental Methodology for Erosion Prediction," *Wear,* vol. 332-333, pp. 1090–1097, 2015.

[2] M. Parsi, K. Najmi, F. Najafifard, S. Hassani, B. S. McLaury and S. A. Shirazi, "A Comprehensive Review of Solid Particle Erosion Modeling for Oil and Gas Wells and Pipelines Applications," *Journal of Natural Gas Science and Engineering,* vol. 21, pp. 850-873, 2014.

[3] T. Frosell, M. Fripp and E. Gutmark, "Investigation of Slurry Concentration Effects on Solid Particle Erosion Rate for an Impinging Jet," *Wear,* vol. 342-343, pp. 33-43, 2015.

[4] I. Finnie, "The Mechanism of Erosion of Ductile Metals," in *3rd U.S. Nat. Congress of Applied Mechanics,* New York, 1958.

[5] R. Bellman and A. Levy, "Erosion Mechanism in Ductile Metals," *Wear,* vol. 70, pp. 1-28, 1981.

[6] V. Sooraj and V. Radhakrishnan, "Elastic Impact of Abrasives for Controlled Erosion in Fine Finishing of Surfaces," *ASME J. Manuf. Sci. Eng.,* vol. 135, pp. 051019-051021, 2013.

[7] M. Liebhard and A. Levy, "The Effect of Erodent Particle Characteristics on the Erosion of Metals," *Wear,* vol. 151, pp. 151-162, 1991.

[8] B. Gandhi and S. Borse, "Effect of Particle Size and Size Distribution on Estimating Erosion Wear of Cast Iron in Sand-Water Slurries," *Indian J. Eng. Mater. Sci.,* vol. 9, pp. 480-486, 2002.

[9] G. Desale, B. Gandhi and S. Jain, "Particle Size Effects on the Slurry Erosion of Aluminum Alloy (Aa 6063)," *Wear,* vol. 266, no. 11-12, pp. 1066-1071, 2009.

[10] A. Levy and P. Chik, "The Effect of Erodent Composition and Shape on the Erosion of Steel," *Wear,* vol. 89, pp. 151-162, 1983.

[11] J. Latoine, "Aerodynamic Effect in the Erosion Process," *Wear,* vol. 56, pp. 239-246, 1979.

[12] J. Latoine, "Erosion Prediction Near the Stagnation Point Resulting from Aerodynamically Entrained Solid Particles," *Journal of Aircraft,* vol. 16, pp. 809-814, 1979.

[13] A. Burnett, S. De Silva and A. Reed, "Comparison between Sand Blast and Centripetal Effect Accelerator Type Erosion Testers," in *8th International Conference on Erosion by Liquid and Solid Impact*, 1994.

[14] C. Smeltzer, M. Gulden and W. Cumpton, "Mechanisms of Metal Removal by Impacting Dust Particles," *Journal of Basic Engineering Transactions,* vol. 92, no. 3, pp. 639-652, 1970.

[15] Y. Oka, K. Okamura and T. Yoshida, "Practical Estimation of Erosion Damage Caused by Solid Particle Impact: Part 1: Effects of Impact Parameters on a Predictive Equation," *Wear,* vol. 259, no. 1-6, pp. 95-101, 2005.

[16] Y. Oka and T. Yoshida, "Practical Estimation of Erosion Damage Caused by Solid Particle Impact: Part 2: Mechanical Properties of Materials Directly Associated with Erosion Damage," *Wear,* vol. 1-6, pp. 102-109, 2005.

[17] G. Sheldon, "Similarities and Differences in the Erosion Behavior of Materials," *ASME J. Basic Eng. Trans.,* pp. 619-626, 1970.

[18] D. Andrews and N. Horsfield , "Particle Collisions in the Vicinity of an Eroding Surface," *Journal of Physics D: Applied Physics,* vol. 16, no. 4, pp. 525-538, 1984.

[19] T. Deng, A. Chaudhry, M. Patel, I. Hutchings and M. Bradley, "Effect of Particle Concentration on Erosion Rate of Mild Steel Bends in a Pneumatic Conveyor," *Wear,* vol. 258, no. (1-4), pp. 480-487, 2005.

[20] I. Finnie, "Erosion of Surfaces by Solid Particles," *Wear,* vol. 3, no. 2, pp. 87-103, 1960.

[21] M.-H. Wang, C. Huang, K. Nandakumar, P. Minev, J. Lou and S. Chiovelli, "Computational Fluid Dynamics Modelling and Experimental Study of Erosion in Slurry Jet Flows," *International Journal of Computational Fluid Dynamics,* vol. 23, no. 2, pp. 155-172, 2009.

[22] S. Turenne, M. Fiset and M. Jacques, "The Effect of Sand Concentration on the Erosion of Materials by a Slurry Jet," *Wear,* vol. 133, no. 1, pp. 95-106, 1989.

[23] L. Giourntas, T. Hodgkiess and A. Galloway, "Comparative Study of Erosion-Corrosion Performance on a Range of Stainless Steels," *Wear,* vol. 332-333, pp. 1051-1058, 2015.

[24] J. Bitter, "A Study of Erosion Phenomena Part I," *Wear,* vol. 6, no. 1, pp. 5-21, 1963.

[25] J. Bitter, "A Study of Erosion Phenomena: Part II," *Wear,* vol. 6, no. 3, pp. 169-190, 1963.

[26] I. Finnie, "Some Observations on the Erosion of Ductile Metals," *Wear,* vol. 19, no. 1, pp. 81-90, 1972.

[27] G. Sheldon and A. Kanhere, "An Investigation of Impingement Erosion Using Single Particles," *Wear,* vol. 21, no. 1, pp. 195-209, 1972.

[28] G. Tilly, "A Two Stage Mechanism of Ductile Erosion," *Wear,* vol. 23, no. 1, pp. 87-96, 1973.

[29] W. Jennings, W. Head and C. Manning Jr., "A Mechanistic Model for the Prediction of Ductile Erosion," *Wear,* vol. 40, no. 1, pp. 93-112, 1976.

[30] I. Hutchings, R. Winter and J. Field, "Solid Particle Erosion of Metals: The Removal of Surface Material by Spherical Projectiles," *Proceedings of the Royal Society of London. Series A, Mathematical and Physical Sciences,* vol. 348, pp. 370-392, 1976.

[31] I. Hutchings, "A Model for the Erosion of Metals by Spherical Particles at Normal Incidence," *Wear,* vol. 70, no. 3, pp. 269-281, 1981.

[32] A. Evans, M. Gulden and M. Rosenblatts, "Impact Damage in Brittle Materials in the Elastic-Plastic Response Regime," *Proceedings of the Royal Society of London. Series A, Mathematical and Physical Sciences,* vol. 361, no. 1706, pp. 343-365, 1978.

[33] W. Tabakoff, R. Kotwal and A. Hamed, "Erosion Study ff Different Materials Affected by Coal Ash Particles," *Wear,* vol. 52, no. 1, pp. 161-173, 1979.

[34] G. Sundararajan and P. Shewmon, "A New Model for the Erosion of Metals at Normal Incidence," *Wear,* vol. 84, no. 2, pp. 237-258, 1983.

[35] G. Sundararajan, "A Comprehensive Model for the Solid Particle Erosion of Ductile Materials," *Wear,* vol. 149, no. (1-2), pp. 111-127, 1991.

[36] A. Venougopal Reddy and G. Sundararajan, "Erosion Behaviour 0f Ductile Materials with a Spherical Non-Friable Erodent," *Wear,* vol. 111, no. 3, pp. 313-323, 1986.

[37] S. Johansson, F. Ericson and J. Schweitz, "Solid Particle Erosion - A Statistical Method for Evaluation of Strength Properties of Semiconducting Materials," *Wear,* vol. 115, no. (1-2), pp. 107-120, 1987.

[38] K. Ahlert, "Effect of Particle Impingement Angle and Surface Wetting on Solid Particle Erosion of AISI 1018 Steel (M.Sc. Thesis)," Department of Mechanical Engineering, The University of Tulsa, Tulsa, 1994.

[39] Y. Zhang, E. Reuterfors, B. McLaury, S. Shirazi and E. Rybicki, "Comparison of Computed and Measured Particle Velocities and Erosion in Water and Air Flows," *Wear,* vol. 263, pp. 330-338, 2007.

[40] B. Levin, K. Vecchio and A. Marder, "Modeling Solid-Particle Erosion of Ductile Alloys," *Metallurgical and Materials Transactions A,* vol. 30, pp. 1763-1774, 1999.

[41] C. Wong, Y. Wu, A. Zamberi, C. Solnordal and L. Graham, "Sand Erosion Modelling," in *SPE Asia Pacific Oil and Gas Conference and Exhibition, Society of Petroleum Engineers,* 2010.

[42] A. Mansouri, S. Shirazi and B. McLaury, "Experimental and Numerical Investigation of the Effect of Viscosity and Particle Size on the Erosion Damage Caused by Solid Particles," in *ASME 2014 4th Joint US-European Fluids Engineering Division Summer Meeting collocated with the ASME 2014 12th International Conference on Nanochannels, Microchannels, and Minichannels,* Chicago, 2014.

[43] V. Nguyen, Q. Nguyen, Z. Liu, S. Wan, C. Lim and Y. Zhang, "A Combined Numerical–Experimental Study on the Effect of Surface Evolution on The Water–Sand Multiphase Flow Characteristics and the Material Erosion Behavior," *Wear*, vol. 319, no. 1/2, pp. 96-109, 2014.

[44] S. Li, J. Humphrey and A. Levy, "Erosive Wear of Ductile Metals by a Particle-Laden High Velocity Liquid Jet," *Wear*, vol. 73, no. 2, pp. 295-309, 1981.

[45] A. Mansouri, M. Mahdavi, S. Shirazi and B. McLaury, "Investigating the Effect of Sand Concentration on Erosion Rate in Slurry Flows," in *NACE International Corrosion 2015 Conference and Expo*, Dallas, 2015.

[46] H. S. Grewal, H. Singh and Eui-Sung Yoon, "Interplay between Erodent Concentration and Impingement Angle For Erosion in Dilute Water–Sand Flows," *Wear*, vol. 332-333, pp. 1111-1119, 2015.

[47] ANSYS, "ANSYS CFX-Solver Theory Guide," ANSYS, Inc., Pennsylvania, 2011.

[48] ANSYS, "ANSYS CFX-Solver Theory Guide," ANSYS, Inc., Pennsylvania, 2015.

[49] S. Dosanjh and J. Humphrey, "The Influence of Turbulence C on Erosion by a Particle Laden Fluid Jet," *Wear*, vol. 102, pp. 309-330, 1985.

[50] I. Hutchings, "Mechanical and Metallurgical Aspects of the Erosion of Metals," in *Conference on Corrosion-Erosion of Coal Conversion System Materials, NACE*, 1979.

Appendix A

All presented codes in this Appendix were developed using MATLAB software.

A.1. Eroded Thickness Averaging

```
clc
clear all
close all

%% Calculating r and Thickness from exported data:
Data=xlsread(NameofDataFile.xlsx');
x=Data(:,1)*10^3;
y=Data(:,2)*10^3;
Thickness=Data(:,3)*10^6;
k=1;
j=1;

for i=1:length(y)
    if (y(i)>=0)
        r_pos(k)=sqrt(x(i)^2+y(i)^2);
        Thickness_pos(k)=Thickness(i);
        k=k+1;
    elseif (y(i)<0)
        r_neg(j)=sqrt(x(i)^2+y(i)^2);
        Thickness_neg(j)=Thickness(i);
        j=j+1;
    end
end

r_neg=rot90(r_neg,2); %Rotating to make the mtx. neg to pos
Thickness_neg=rot90(Thickness_neg,2);
r=[-(r_neg');r_pos'];
Th_new=[Thickness_neg';Thickness_pos'];
% plot(r,Th_new,'r-o');

%% Calculating average thickness at every radius:
r_c=10000;
k=1;
n=1;

for i=1:length(r)
    if((abs(r_c)>abs(r(i))+0.001)||(abs(r_c)<abs(r(i))-0.001))
        r_c=r(i);
        for j=1:length(r)

      if((abs(r_c)<=abs(r(j))+0.001)&&(abs(r_c)>=abs(r(j))-0.001))
                Th_new2(k,n)=Th_new(j);
                n=n+1;
            end
        end
        n=1;
        r_final(k,1)=r_c;
        k=k+1;
    end
end

for i=1:k-1
```

```
    if((r_final(i)>0.001)||(r_final(i)<-0.001))
        Th_final(i,1)=mean(Th_new2(i,:));
    else
        Th_final(i,1)=Th_new2(i,1);
    end
end

Th_final=-Th_final;
plot(r_final,Th_final,'ro-','linewidth',1.5);
xlabel('Radius(mm)');
ylabel('Eroded Thickness(microns)');
title('Erosion Profile - Finnie Model');
% title('Eroded Thickness on Coupon Surface');
axis([-12 12 -145 0]);
```

A.2. Particle Velocity Components Averaging

```
clc
clear all
close all


%% Calculating r and Organizing Velocity from exported data:
ch=input('Please input 1 for u or 2 for v or 3 for w:\n');
Data=xlsread(NameofDataFile.xlsx');
x=Data(:,1)*10^3;
y=Data(:,2)*10^3;
if ch==1
    Velocity=Data(:,3);
    Velocity=abs(Velocity);
elseif ch==2
    Velocity=Data(:,4);
    Velocity=abs(Velocity);
else
    Velocity=Data(:,5);
end

k=1;
j=1;

for i=1:length(y)
    if (y(i)>=0)
        r_pos(k)=sqrt(x(i)^2+y(i)^2);
        Velocity_pos(k)=Velocity(i);
        k=k+1;
    elseif (y(i)<0)
        r_neg(j)=sqrt(x(i)^2+y(i)^2);
        Velocity_neg(j)=Velocity(i);
        j=j+1;
    end
end

r_neg=rot90(r_neg,2); %Rotating to make the mtx. neg to pos
Velocity_neg=rot90(Velocity_neg,2);
r=[-(r_neg');r_pos'];
Velocity_new=[Velocity_neg';Velocity_pos'];

%% Calculating Average Velocity at Every Radius:
r_c=10000;
k=1;
```

```
n=1;

for i=1:length(r)
    if((abs(r_c)>abs(r(i))+0.001)||(abs(r_c)<abs(r(i))-0.001))
        r_c=r(i);
        if ch==3 %Ensuring to average only -ve w-velocites
            for j=1:length(r)

      if((abs(r_c)<=abs(r(j))+0.001)&&(abs(r_c)>=abs(r(j))-0.001))
                    if (Velocity_new(j)<=0)
                        Velocity_new2(k,n)=Velocity_new(j);
                        n=n+1;
                    else
                        Velocity_new2(k,n)=0;
                        n=n+1;
                    end
                end
            end
        else
            for j=1:length(r)

      if((abs(r_c)<=abs(r(j))+0.001)&&(abs(r_c)>=abs(r(j))-0.001))
                    Velocity_new2(k,n)=Velocity_new(j);
                    n=n+1;
                end
            end
        end
        n=1;
        r_final(k,1)=r_c;
        k=k+1;
    end
end

for i=1:k-1
    if((r_final(i)>0.001)||(r_final(i)<-0.001))
        Velocity_final(i,1)=mean(Velocity_new2(i,:));
    else
        Velocity_final(i,1)=Velocity_new2(i,1);
    end
end

hold on
plot(r_final,Velocity_final,'r*','linewidth',1.5);
xlabel('Radius(mm)');
ylabel('Average Velocity(m/s)');
if ch==1
    title('u-Average Velocity at Coupon Surface');
elseif ch==2
    title('v-Average Velocity at Coupon Surface');
else
    title('w-Average Velocity at Coupon Surface');
end
xlim([-12 12]);
```

A.3. Calculating Average Particle Impact Velocities and Angles, Function of Impact Angle, and Erosion Profile

```
clc
clear all
```

```
close all

%% Importing Velocity Data and Plotting Them:
Data=xlsread(NameofDataFile.xlsx');
r=Data(:,1);
u=Data(:,2);
v=Data(:,3);
w=Data(:,4);

figure(1)
hold on
plot(r,u,'ro','linewidth',1.5);
plot(r,v,'b^','linewidth',1.5);
plot(r,w,'k*','linewidth',1.5);
xlabel('Radius(mm)');
ylabel('Sand Average Velocity(m/s)');
title('Sand Average Velocity at Coupon Surface');
legend('u','v','w');
xlim([-13 13]);
% axis([-13 13 -0.5 0.5]);
hold off



%% Calulating Impact Velocity and Angle:
k=1;

for i=1:length(r)

        V_xy(k,1)=sqrt(u(i)^2+v(i)^2);
        V_R(k,1)=sqrt(w(i)^2+V_xy(k,1)^2); %Resultant impact velocity
    Alpha_rad(k,1)=atan(abs(w(i))/V_xy(k,1)); %Resultant impact angle
        Alpha(k,1)=Alpha_rad(k,1)*180/pi; %Converting to degrees
        if tan(Alpha_rad(k,1))>(1/3)
            f_alpha(k,1)=(1/3)*(cos(Alpha_rad(k,1)))^2;
        else
            f_alpha(k,1)=sin(2*Alpha_rad(k,1))-
3*(sin(Alpha_rad(k,1)))^2;
        end
   ER(k,1)=((V_R(k,1)/2300)^(2.4))*f_alpha(k,1); %Finnie Model in CFX
        ER(k,1)=-ER(k,1); %Converting results to -ve values
        rr(k,1)=r(i);
        k=k+1;

end

figure(2)
subplot(1,2,1)
plot(rr,V_R,'r*','linewidth',1.5);
xlabel('Radius(mm)');
ylabel('Impact Velocity(m/s)');
xlim([-13 13]);
title('Average Impact Velocity');

subplot(1,2,2)
plot(rr,Alpha,'b*','linewidth',1.5);
xlabel('Radius(mm)');
ylabel('Impact Angle(degree)');
xlim([-13 13]);
title('Average Impact Angle');
```

```
figure(3)
subplot(1,2,1)
plot(Alpha,f_alpha,'r-','linewidth',1.5);
xlabel('Impact Angle(degree)');
ylabel('Function of Impact Angle');
title('Average Function of Impact Angle');

subplot(1,2,2)
plot(rr,-(ER./min(ER)),'b-','linewidth',1.5); %Normalizing ER
xlabel('Radius(mm)');
ylabel('Normalized Erosion Ratio');
xlim([-13 13]);
title('Average Dimensionless Erosion Profile');
```

Vita

Wahib Mufid Salim is a Syrian who was born in 1993, in Sharjah, United Arab Emirates. He received his B.Sc. degree in Mechanical Engineering from the American University of Sharjah in 2014.

In September 2014, he joined the Mechanical Engineering master's program in the American University of Sharjah as a graduate research assistant. During his master's study, he worked as a research and teaching assistant in addition to co-authoring 2 academic papers. His research interests are in the areas of fluid mechanics, and kinematics and dynamics.